Model Calculations on One-Dimensional (1D) Poly-Decker Sandwich Compounds. A Crystal Orbital Investigation Based on the Tight-Binding Formalism

Michael C. Böhm

Max-Planck-Institut für Festkörperforschung, Stuttgart

Z. Naturforsch. **39a**, 223–246 (1984); received December 2, 1983

The band structures of 11 one-dimensional (1D) poly-decker sandwich compounds with different transition metal centers M (M = Mn, Fe, Co, Ni, Cu, Zn) and a variety of fivemembered π ligands L from the cyclopentadienyl moiety (C_5H_5) to the pure boron ring B_5H_5 have been studied by means of a semiempirical crystal orbital procedure based on the INDO approximation in order to allow a priori predictions on possible semiconducting or conducting low-dimensional materials composed by ML fragments. To determine the (numerically) different self-energy corrections (i.e. long-range and short-range "correlations") in the transition metal 3d spines and the ligand backbones approximate quasi-particle shifts have been employed for the correction of the Hartree-Fock (HF) band energies. The band structure properties (e.g., dispersion curves, density of states distributions, effective mass parameters, propagation times of charge carriers) are discussed in the light of the semiempirical tight-binding approach. It is shown that the forbidden band gaps are reduced with an increasing number of B atoms in the π ligands. The gap in the $Mn(C_5H_5)$ stack amounts to 8.27 eV, while overlapping dispersion curves are predicted in the $Zn(B_5H_5)$ derivative. This model polymer is the only intrinsic conductor in the series of the studied 1D metallocenes; all other compounds require injected charge carriers (electrons or holes) in order to achieve partially filled bands. Injected holes in the Mn or Fe backbones lead to 1D materials with conducting 3d spines; the charge transfer in this regime is best described as some type of hopping motion. The remaining poly-decker strands belong to the class of organic metals (injected carriers) with conductive pathways that are formed by diffuse ligand states leading to transfer processes that can be rationalized in terms of a band picture. The rotational profiles and the magnitudes of intracell and intercell interactions are also studied. The band structure properties (band gaps, characters of the valence and conduction bands) depend critically on the mutual orientations between neighbouring unit cells in the case of ligands with low spatial symmetries. General rules and strategies for synthetic approaches to organometallic 1D materials containing 3d centers with small or vanishing band gaps are formulated.

1. Introduction

The chemical and physical properties of low-dimensional transition metal compounds with organometallic unit cells have been investigated in large detail in the last years [1–4]. It has been shown that these one-dimensional (1D) stacks show often semiconducting or even conducting properties in the solid state. The variety of organometallic 1D systems can be roughly divided into four large groups on the basis of the topological arrangement of the different stacking units. Simplified representations of the mutual coupling schemes are summarized in Figure 1. Direct metal-metal contacts are found within the columnar structures of the class **A** materials with planar organometallic units that are stacked metal-over-metal. An angle of 90° is formed between the ligand plane and the longitudinal axis. Deviations from the 90° arrangement are encountered in the polymers of class **B** with short metal-ligand contacts between adjacent moieties. The 1D systems of class **A** are often called M–M phases, while the slipped arrangements are characterized as M–L–M modifications [5]. The transition metal atoms in 1D materials of class **C** are separated by the organic ligands or by bridging fragments –X–. The stacking units are thus coupled via metal-ligand bonds. The organometallic polymers of class **D**, at least, are formed by building blocks connected via covalent ligand-ligand interactions.

The current experimental activities in the field of 1D organometallics of the classes **A**–**D** were restricted to a limited number of model compounds. The tetracyano platinate chain $(K_2[Pt(CN)_4]Br_{0.3}$

Reprint requests to Dr. M. C. Böhm, Max-Planck-Institut für Festkörperforschung, Heisenbergstr. 1, D-7000 Stuttgart 80, West-Germany.

0340-4811 / 84 / 0300-0223 $ 01.3 0/0. – Please order a reprint rather than making your own copy.

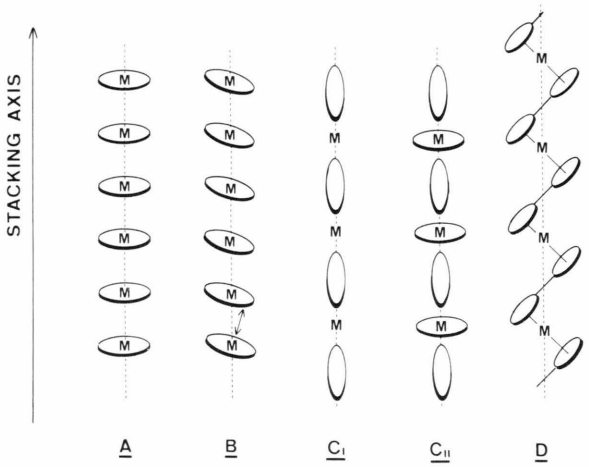

Fig. 1. Simplified representation of the four topologically different types of one-dimensional (1D) transition metal polymers **A**, **B**, **C** ($\mathbf{C}_I$ and $\mathbf{C}_{II}$) and **D**, respectively, that can be discriminated on the basis of the intercell coupling between the molecular building blocks. The type **A** materials crystallize in the form of columnar structures with a metal-over-metal arrangement. The angle between the stacking axis and the mean plane of the organic ligand is 90°. Polymers of class **B** show a slipped arrangement with respect to the stacking direction. The angle between the 1D axis and the ligand plane differs from the perpendicular 90° orientation. The shortest intercell contacts are found between the metal center (M) of one unit cell and ligand atoms in the nearest neighbouring moieties. The transition metal atoms of class **C** ($\mathbf{C}_I$ and $\mathbf{C}_{II}$) chains are separated by organic ligands or bridging atoms. $\mathbf{C}_I$ and $\mathbf{C}_{II}$ differ with respect to the environment around the transition metal centers. In the first backbone the metal atoms are only coupled to ligand units in the direction of the longitudinal axis (e.g.: tetrathiosquarato nickel(II)). In the 1D stacks of the latter topology the metal sites M belong to planar organometallic building blocks with vacant positions in the direction of the 1D axis; in the polymer chain these vacancies are occupied by organic π ligands or bridging atoms. Both polymer units ($\mathbf{C}_I$ and $\mathbf{C}_{II}$) are thus coupled via covalent metal-ligand bonds. The 1D materials of class **D** are characterized due to ligand-ligand bonds between neighbouring stacking fragments.

$\cdot 3H_2O$, Krogmann's salt) is a historically important example for a highly conducting material in the 1D backbones with columnar structures (**A**) [6]. Porphyrin derivatives and phthalocyanine materials on the other side have focused most of the very recent experimental interest in this group of low-dimensional transition metal derivatives [2]. Highly conducting organometallics, that crystallize in the M–L–M modification **B**, are yet not known. On the other side, it has been demonstrated that the insulating (undoped) modifications of partially oxidized (doped) conducting chains of class **A** favour often the crystallization in the stacking pattern **B** in the absence of oxidants [2]. Some typical representatives of class **C**, that have been investigated by experimental groups, are tetrathiosquarato nickel(II) [7], phthalocyanine stacks with SiO, GeO or SnO bridges [8] as well as metallomacrocycles with 3d transition metal centers that are coupled by means of organic π systems [9, 10]. At the end, we want to mention the large number of low-dimensional polyferrocenylene derivatives that belong to the 1D stacks with ligand-ligand bonds (**D**) between the molecular fragments [11, 12]. It is common to all these organometallic polymers that they are insulators in the absence of materials leading to a partial oxidation or reduction (i.e. to nonintegral oxidation states due to an incomplete charge transfer).

It had been mentioned that the recent experimental activities towards conducting or semiconducting transition metal polymers were restricted to a limited set of model systems. Therefore, it is not astonishing that there exists a vital interest to synthesize and characterize new 3d materials with metallic or semimetallic properties in the solid state. In the molecular field it has been shown that possible synthetic strategies towards systems with specific properties can be often guided and facilitated by quantum chemical model investigations. Such an interplay of theory and experiment is yet not found in the solid state area. This deficit must be traced back to the complicated structure of the low-dimensional materials on one side and the elaborate computational expenditure of reliable theoretical solid state models on the other side. Previous experience, e.g., has shown that simplified one-electron procedures (Wolfsberg-Helmholtz or Extended Hückel Hamiltonians) are often too insensible to allow a priori predictions about conducting or insulating properties of 1D derivatives, the possibility of band conductivities or diffusive hopping processes etc. [13–15]. These shortcomings of simple one-electron procedures are of course expected, as the classical contributions of Mott and Slater have shown that it is the electron-electron interaction that determines whether a solid is an insulator, a semiconductor or a conductor [16, 17].

In order to allow theoretical investigations on extended metallomacrocycles in the framework of the Hartree-Fock (HF) approximation, we have developed a semiempirical crystal orbital (CO) formalism [18] which is based on the tight-binding formal-

ism for infinite periodic systems with cyclic boundary conditions [19, 20]. The employed CO scheme is formulated in the framework of the well-known CNDO or INDO approximation in the ZDO (zero differential overlap) hierarchy. The self-consistent-field (SCF) HF CO procedures have been derived to reproduce the results of timeconsuming ab initio calculations in the framework of dressed ZDO operators with screened two-electron parameters [21]. We have used this CO method to study the solid state properties (e.g., band structures $\varepsilon(k)$, density of states distributions $N(E)$, nature of intracell and intercell interactions, geometrical effects in the solid state, transfer paths and transport mechanisms of (injected) charge carriers, etc.) of a large number of recently synthesized transition metal polymers of the classes **A**–**D** as well as of organic donor-acceptor systems [22, 23]. In the type **A** materials we have analyzed the solid state electronic structures of bis(glyoximato)nickel(II) [24], bis(benzoquinonedioximato)nickel(II) [25], Ni(II) porphyrinato and tetraza porphin stacks [26–28]. The slipped modification of bis(glyoximato)-nickel(II) has been investigated as a representative example in the class **B** backbones with short metal-ligand contacts between neighbouring unit cells [29]. In the case of low-dimensional materials with covalent metal-ligand-metal bonds we have considered the above mentioned systems tetrathiosquarato nickel(II) [30], bis(glyoximato)pyrazine iron(II) [31] as well as tetraza porphin moieties with SiO and GeO bridges [32]. The band structure of polyferrocenylene has been examined to understand and to file the solid state properties of class **D** polymers [33]. The HF SCF INDO CO investigations on organic and transition metal backbones allowed in any case the interpretation of a large amount of experimental results. The dressed nature of the HF SCF CO Hamiltonian even made possible reliable predictions of optical band gaps as a result of the renormalization of the two-electron part in the HF operator and the screening of the one-particle regime (i.e. occupied and empty Fermi seas) [34–37]. The screened electron-electron interaction terms diminish furthermore the shortcomings of the HF potential to describe the virtual one-particle space by means of a V_N (N electron system) potential instead of the physically justified $V_{(N-1)}$ potential [38, 39].

The successful application of the semiempirical HF SCF INDO CO formalism to a large number of organometallic polymers suggests to employ this method also to investigate systematically solid state properties of low-dimensional materials, where also unexpected physical and chemical properties can be expected, and thus to allow a priori predictions of suitable precursors and synthetic routes. It is the purpose of the present contribution to analyze the band structures of one-dimensional metallocene (multiple-decker) derivatives (see Fig. 2) with an alternating arrangement of fivemembered homo- and heterocyclic π ligands L and transition metal atoms M that form unit cells with 12 (or 14) outer valence electrons (only the ligand π and metal 3d electrons are counted). The molecular building blocks of the 1D materials summarized in Fig. 2 have been stud-

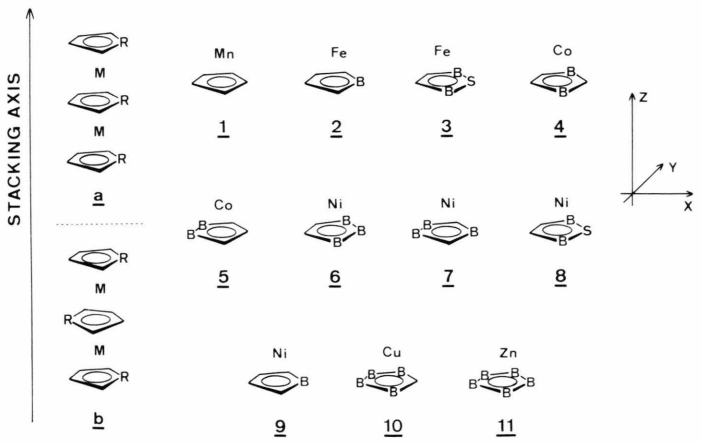

Fig. 2. Schematic representation of the molecular stacking units **1**–**11** that are studied in the present investigation. On the left side of the figure we have displayed the 1D arrangement for the eclipsed conformation with a torsional angle of 0° between direct neighbours (**a**) and the staggered orientation (**b**). In the latter stacking pattern a mutual torsional angle of 180° is found between adjacent unit cells. The employed coordinate system for the 1D materials is shown on the extreme right.

ied extensively in the last years (i.e.: triple-decker and tetra-decker sandwiches with a large variety of heteroligands and 3d atoms) [40–42].

The extension of recent synthetic activities from finite clusters to 1D systems seems to be rather attractive as detailed experimental and theoretical studies on the molecular building blocks have shown a high degree of charge delocalization in some ions of the multiple-decker sandwiches; the transition metal fragments are thus not electronically isolated from each other [41, 43]. This behaviour is obviously a necessary condition for high conductivities in the solid state.

The following theoretical aspects will be discussed in detail in the present investigation to the collection **1–11** of 1D stacks that belong all to class **C**: a) Dependence of the band structures and density of states distributions as a function of the 3d centers and the organic π ligands; most of the cyclic moieties summarized in Fig. 2 are well-known ligand fragments employed in experimental approaches to poly-decker sandwich compounds*. b) Discrimination into intrinsic conductors with partially filled bands even in the absence of electron donors or acceptors and charge transfer systems that require oxidizing or reducing species in conducting modifications. c) Discrimination into organic metals with ligand states that form the conductive pathways and conducting transition metal derivatives, where the charge transfer channels are formed by the 3d spines. d) On the basis of the CO results it will be possible to separate the 1D stacks into systems where the charge transport can be described within a band model, and materials that belong to the large group of polaronic conductors with transport processes of the hopping type between localized states. e) Formulation of general rules that allow one to estimate those topological and structural factors favouring or suppressing the formation of small (or vanishing) band gaps.

Quantum chemical investigations on simple metallocene derivatives either by means of semiempirical or ab initio LCAO methods are legion and can not be reviewed in this context. The bonding capabilities of conical ML fragments have been discussed on the basis of one-electron calculations of the EH type [44]. The first computational approach to triple-decker sandwiches was also based on the EH Hamiltonian [45]. The importance of electron-electron interactions had been demonstrated in subsequent theoretical model studies [41] that were based on the semiempirical HF SCF INDO Hamiltonian of [21] or that were even beyond the mean-field description of the HF scheme [43].

The plot of the present manuscript is as follows: The computational background of the semiempirical crystal orbital model is shortly summarized in the following section. Here also those theoretical steps beyond the HF scheme are discussed that are necessary for a critical analysis of the band structure data. We will adopt approximate elements of the quasi-particle approach to estimate the importance of long-range and short-range correlations and relaxations in the 1D stacks. The computational results are presented in Sect. 3 and are analyzed in Paragraph 4.

2. Theoretical Background and Computational Conditions

The theoretical background of the crystal orbital formalism has been described in the literature [19, 20] and is thus not reviewed in detail in this context. The state of art of tight-binding procedures [46–48] as well as computational shortcomings of the method [49] have been reviewed thoroughly in previous contributions. The combination of the variational HF scheme with the translational symmetry encountered in an infinite 1D backbone leads to a set of coupled, complex Hermitian pseudoeigenvalue equations that are defined in (1) in the ZDO adapted form.

$$F(k)\,C(k) = \varepsilon(k)\,C(k)\,; \tag{1}$$

k is of course the convenient wave vector in solid state theory characterizing the translational symmetry. $F(k)$ is the k-dependent Fock operator given by the Fourier sum of (2); the $C(k)$ set symbolizes the variational coefficients of the crystal orbitals and the $\varepsilon(k)$'s are one-electron energies forming the dispersion curves of the low-dimensional material within the mean-field (HF) approximation.

$$F(k) = \sum_{j=-\infty}^{+\infty} \exp(i\,j\,k)\,F(j)\,; \tag{2}$$

j in (2) is a cell index that labels the building blocks in the 1D stack ($j = 0$, reference cell in the origin). The matrix elements of the Fock operator in the

* The systems **5**, **6**, **7**, **10** and **11**, respectively, have been postulated as suitable ligand fragments.

semiempirical INDO approximation are defined in [18]. The k-dependent eigenvalue problems of (1) are coupled by means of the charge-density-bond-order matrix $P(j-j')_{\mu\nu}$ which has to be calculated via a numerical integration within the first Brillouin zone.

$$P(j-j')_{\mu\nu} = (c/2\pi) \int_{-\pi/c}^{+\pi/c} \sum_i c^*_{\mu ik}\, c_{\nu ik} \cdot \exp\left[ik(j-j')\right] \Theta(\varepsilon_F - \varepsilon_i(k))\, dk\,; \tag{3}$$

μ and ν symbolize atomic orbital (AO) basis functions and c is the unit cell dimension of the polymer. The summation over i is controlled by the Heaviside step function $\Theta(\varepsilon_F - \varepsilon_i(k))$, see (4), where ε_F is the Fermi energy.

$$\begin{aligned} &\Theta(\varepsilon_F - \varepsilon_i(k)) = 1, \quad \varepsilon_i(k) \leqq \varepsilon_F\,; \\ &\Theta(\varepsilon_F - \varepsilon_i(k)) = 0, \quad \varepsilon_i(k) > \varepsilon_F\,. \end{aligned} \tag{4}$$

The total energy of the 1D system is defined in (5); $E^{HF}_{TOT}(N)$ has been normalized to one unit cell. $H(k)$ stands for the one-electron part of the Fock operator and E_{CC} is the core-core repulsion in the 1D system.

$$E^{HF}_{TOT}(N) = (c/2\pi) \int_{-\pi/c}^{+\pi/c} \sum_i \sum_\mu \sum_\nu \cdot \left[c^*_{\mu ik}\,(H(k) + F(k))\, c_{\nu ik}\right] \cdot \Theta(\varepsilon_F - \varepsilon_i(k))\, dk + E_{CC}\,. \tag{5}$$

In order to simplify the analysis of the subsequent results, we make use of partitioning schemes that lead to a straightforward fragmentation of $E^{HF}_{TOT}(N)$ into terms of physical significance. $E^{HF}_{TOT}(N)$ can be decomposed into the total intracell energy (E_{INTRA}) as well as into intercell elements (E_S) that offer quantitative insight into the coupling strength between the building blocks in the 1D arrangement.

$$E^{HF}_{TOT}(N) = E_{INTRA} + E_S\,. \tag{6}$$

In the following we want to restrict our interest to the intercell terms E_S that can be divided into resonance energies (E_{RES}), that are a measure for the covalent interaction between the various atomic sides (kinetic energy operator), into an exchange element, that describes the Fermi correlation due to the antisymmetry of the one-determinant in the HF approximation and into the classical Coulomb energy (E_{COU}) which is given by the sum of electron-electron repulsion, electron-core attraction and the repulsion between the atomic cores. In ZDO based models it is always possible to reduce these parameters to two-center couples between the atoms A and B E^{AB}_{RES}, E^{AB}_{EX}, and E^{AB}_{COU}, respectively [50]. Thus the following equations are valid in ZDO based CO calculations to define the intercell energies in the 1D stack.

$$E_S = \sum_j E_{RES} + E_{EX} + E_{COU}\,, \tag{7}$$

$$E_S = \sum_j \sum_{A_0} \sum_{B_j} E_{A_0 B_j}\,, \tag{8}$$

$$E_{A_0 B_j} = E^{AB}_{RES} + E^{AB}_{EX} + E^{AB}_{COU}\,. \tag{9}$$

The band energies $\varepsilon_i(k)$ can be related to auxiliary functions that characterize the physical conditions experienced by injected carriers (electrons and holes). In (10) we have displayed simple effective mass relations (m_h, m_e) derived by means of a k-averaged parabolic energy wave vector connection [51]. The m_h or m_e figures are an indicator for deviations of the charge carriers from the free electron behaviour.

$$m_{h(e)} = (\hbar^2 \pi^2)/(2c^2 \Delta\varepsilon_{v(c)})\,. \tag{10}$$

$\Delta\varepsilon_v$ and $\Delta\varepsilon_c$ stand for the widths of the valence or conduction bands of the polymer. The parameter T_c in (11) corresponds to the hopping time for an electron or hole from one unit cell of the 1D stack to the nearest neighbouring moiety with the mean group velocity $\bar{v}$. T_c is defined by means of the convenient uncertainty principle and $\bar{v}$ is given in (12) where Δk is the k-interval from the center of the Brillouin zone ($k=0$) to the zone edge ($k=\pi/c$).

$$T_c \Delta\varepsilon \cong \hbar\,, \tag{11}$$

$$\bar{v} = \hbar^{-1}(\Delta\varepsilon/\Delta k)\,. \tag{12}$$

A careful analysis of the T_c numbers provides one with informations on possible electron-lattice interactions (polaron trapping) in the conduction processes [52] and on the importance of short-range reorganizations (electronic relaxation and correlation) accompanying the propagation of the charge carriers (holes or electrons) through the lattice [53 – 56]. The influence of electron-phonon coupling as well as of short-range "relaxations" is obviously enhanced with decreasing group velocities $\bar{v}$ or increasing times of (electron or hole) propagation T_c.

Correlation and relaxation effects are neglected in the band energies $\varepsilon_i(k)$ derived in the HF approximation. Detailed theoretical investigation on molecular building blocks (i.e. 3d complexes), however, have shown that many-body effects play a signifi-

cant role in (weakly coupled) transition metal systems. Thus it has been demonstrated, that Koopmans' theorem [57] is nonvalid to assign low-energy photoelectron spectra of 3d complexes as a result of remarkable relaxation and correlation effects accompanying the ejection of strongly localized 3d electrons [58–61]. ΔSCF calculations on weakly coupled binuclear complexes and diatomic 3d clusters at larger internuclear separations converged into symmetry-broken, localized hole-states [62–64]. These instabilities of the Hartree-Fock solutions demonstrate the crucial importance of left-right correlation between the transition metal centers and can be interpreted as a self-reorganization of the electronic (HF) wave function from the incorrect delocalized MO limit to physically correct VB type functions. Similar effects have been also discussed in low-dimensional transition metal polymers [65]. The various types of correlation effects in 3d systems with differences in the coupling strength have been analyzed thoroughly in previous contributions [43, 66–70]. On the basis of this theoretical material it must be suggested that electronic correlation and relaxation effects in the transition metal spines of the 1D stacks **1**–**11** have also a remarkable control on the electronic structures of these transition metal polymers. Thus it is necessary to take into account electronic reorganizations to decide, whether injected charge carriers in **1**–**11** belong to the transition metal atoms or to ligand states. The third possibility in conducting organometallic polymers is a degeneracy between partially filled 3d and ligand functions (i.e. doubly mixed valence systems).

The physical significance of the Hartree-Fock energy bands is defined in (13) and (14) for the occupied HF space (v) and the empty subspace (c) by means of the well-known Koopmans' theorem.

$$\varepsilon_v(k) = E_{TOT}^{HF}(N) - E_{TOT,v}^{HF}(N-1) = -I_v^{HF}, \quad (13)$$

$$\varepsilon_c(k) = E_{TOT,c}^{HF}(N+1) - E_{TOT}^{HF}(N) = -A_c^{HF}. \quad (14)$$

These relations contain neither short-range nor long-range corrections due to electronic correlations and relaxations in the solid state ensembles. The latter quantities can be taken into account via quasi-particle bands, $\varepsilon_{QP,v}(k)$ and $\varepsilon_{QP,c}(k)$, respectively, that are defined in (15) and (16) by means of the exact energies $E_{TOT}(N)$.

$$\varepsilon_{QP,v}(k) = E_{TOT}(N) - E_{TOT,v}(N-1) = -I_v, \quad (15)$$

$$\varepsilon_{QP,c}(k) = E_{TOT,c}(N+1) - E_{TOT}(N) = -A_c. \quad (16)$$

In solid state theory it is a widely used procedure to relate quasi-particle bands to the HF dispersions by means of perturbational self-energy expansions $\Sigma_{H,v}^{(N-1)}$, $\Sigma_{E,v}^{(N)}$, $\Sigma_{H,c}^{(N)}$ and $\Sigma_{E,c}^{(N+1)}$ that describe the long-range correlations in the infinite materials [53–55, 71]. $\Sigma_{H,v}^{(N-1)}$ is the self-energy of the v-th hole-state, $\Sigma_{E,v}^{(N)}$ is the electron self-energy associated to the valence bands of the (N) electron stack, $\Sigma_{H,c}^{(N)}$ is once again a hole correction for the conduction band, while the last element is the corresponding electron self-energy. The detailed formulas for the determination of these many-body corrections have been reported in the literature [53–55, 71]. The narrow band widths in transition metal polymers of the 3d series as well as the large on-site electron-electron interaction integrals are the physical sources for the fact, that many-body effects are insufficiently described in terms of the aforementioned long-range self-energy parameters [72]. The low group velocities cause strong local (short-range) reorganizations within the stacking units of the infinite materials. It is therefore necessary to consider self-energy corrections for these local reorganization processes; they can be divided into relaxation energies, the loss or gain of ground state correlation due to the variation in the number of electrons and the modification of the electronic correlation as many-body response to orbital relaxation [72]. The theoretical details of this procedure are discussed in large detail in [72]. The relevant formulas for the quasi-particle energies under the inclusion of short-range and long-range corrections are given in (17) and (18), where $M_{H,v}^{(N-1)}$, $M_{E,v}^{(N)}$, $M_{H,c}^{(N)}$, and $M_{E,c}^{(N+1)}$ are the short-range counterparts of $\Sigma_{H,v}^{(N-1)}$, $\Sigma_{E,v}^{(N)}$, $\Sigma_{H,c}^{(N)}$, and $\Sigma_{E,c}^{(N+1)}$, respectively.

$$\begin{aligned}\varepsilon_{QP,v}(k) &= \varepsilon_v(k) + \Sigma_{H,v}^{(N-1)} + \Sigma_{E,v}^{(N)} + M_{H,v}^{(N-1)} + M_{E,v}^{(N)} \\ &= \varepsilon_v(k) + \Delta\varepsilon_{QP,v}; \end{aligned} \quad (17)$$

$$\begin{aligned}\varepsilon_{QP,c}(k) &= \varepsilon_c(k) + \Sigma_{H,c}^{(N)} + \Sigma_{E,c}^{(N+1)} + M_{H,c}^{(N)} + M_{E,c}^{(N+1)} \\ &= \varepsilon_c(k) + \Delta\varepsilon_{QP,c}. \end{aligned} \quad (18)$$

Approximate computational schemes for the determination of the quasi-particle shifts $\Delta\varepsilon_{QP,v}$ and $\Delta\varepsilon_{QP,c}$ have been developed in our previous contribution [72] and will be applied in the following sections to discriminate organic conductors from systems with partially filled metal 3d states. The quasi-particle corrections lead to upwards shifts for the filled energy bands and to the opposite effects for the virtual dispersion curves; the net result is a

reduction of the gap between the occupied and empty Fermi seas in insulating model polymers. It is obvious that these effects are of larger importance in the transition metal (3d) subspace in comparison to the ligand functions that are delocalized over all atomic centers (ligand sides) within the unit cells of the polymers.

The transport properties in conducting polymer modifications are furthermore influenced due to the spatial carrier properties that can be either delocalized in nature or localized. The band description is valid in the first case, while charge transfer processes in the latter case are best described as some type of hole or electron hopping between localized states. These problems have been investigated in some detail by Kunz et al. [65, 73, 74]. Violations of the full translational symmetry (carrier localization) must be expected for those systems where the intracell relaxation energy for the v-th or c-th state exceeds the band width $\Delta\varepsilon_{v(c)}$ of the corresponding dispersion curve [65]. Our previous studies on hole-state properties of transition metal complexes have shown, that this criterion should be extended to the net local reorganizations, i.e. the sum of electronic relaxation and correlation, as the many-body energies are by no means negligible in comparison to orbital relaxation [58, 59, 72]. Thus the relations (19) and (20) can be employed to separate the Bloch conductivity mechanism from hopping events; ΔE_{REG} is the total intracell (short-range) reorganization, which is given by $M_{H,v}^{(N-1)} + M_{E,v}^{(N)}$ in the occupied one-particle space and by $M_{H,c}^{(N)} + M_{E,c}^{(N+1)}$ in the empty Fermi sea.

band conductivity: $|\Delta E_{REG}| \leqq \Delta\varepsilon_{v(c)}$; (19)

hopping conductivity: $|\Delta E_{REG}| > \Delta\varepsilon_{v(c)}$. (20)

In recent contributions we have determined these local reorganization energies [58, 59, 72]. They amount to ca. 2.5−3.0 eV in the case of strongly localized 3d orbitals (Mn, Fe, Co or Ni centers) and are smaller than 0.5 eV in the limit of diffuse ligand functions.

A classical definition via a summation over N_k k-points has been adopted for the determination of the density of states distributions $N(E)$ in the 1D stacks **1**–**11** [75]. We have employed 30000 k-points per $\varepsilon(k)$ curve. This sampling procedure avoids the complicated determination of $(1/\pi)(\partial k/\partial E)$ with all possible singularities and discontinuities. The N_k points have been calculated by means of fourth order polynomials that were determined via a least squares fits to the ten available k-points per band.

The occupation schemes of the various dispersion curves have been settled on the basis of preliminary one-electron calculations of the Extended Hückel type. Often several start occupation patterns (metallic and insulating $\varepsilon(k)$ profiles) have been iterated up to a given SCF criterion. The results summarized in the next sections correspond to those filling schemes that are lowest in energy. To conserve the preselected band occupancies during the iterative circles and to avoid shell swapping between the occupied and empty Fermi seas we have employed an accelerated Hartree damping of the k-dependent charge-density-bond-order matrices 76]. The iterative HF SCF CO steps have been continued until the energy differences between two subsequent steps were smaller than 10^{-4} au.

Our recent crystal orbital studies have shown, that five neighbours should be taken into account in the determination of the lattice sums (index j); this dimension leads to computational results that stabilize the band energies as well as the charge distributions in the 1D systems [24, 25, 33]. Thus all HF SCF INDO CO calculations have been performed in the $j = 5$ array. 10 k-points have been considered for the solutions of (1) and (5), respectively.

We have adopted geometrical parameters for the semiempirical crystal orbital investigations that have been derived by means of X-ray diffraction studies on polynuclear poly-decker sandwich compounds [41, 77, 78]. In each 1D system we have studied the eclipsed orientation (**a**) with a torsional angle α of 0° between neighbouring unit cells as well as the staggered arrangement (**b**) where α amounts to 180°. A standard bond length of 1.10 Å has been adopted for the CH bonds and a value of 1.19 Å for the BH distances [79]. The unit cell dimensions c in the 1D series **1**–**11** are found in an interval from 3.146 Å (**11**) to 3.580 Å (**9**) and have been also transferred from X-ray investigations on the polynuclear building blocks.

3. Results

The density of states distributions of **1**–**11** as determined in the framework of the HF approxima-

tion are displayed in the Figs. 3–13. The $N(E)$ profiles for hole- and particle-states in the interval between −25 eV to 10 eV are shown in these histograms. The employed energy grid amounts to 0.2 eV. We have used separate scale factors for the normalization of the $N(E)$ peaks in the various density of states plots. The associated $\varepsilon(k)$ curves for a representative collection of poly-metallocenes are given in the Figs. 14–19. The model systems **1** and **11** with the fivefold rotational axes in the stacking directions have been selected on one side as well as the 1D materials **4**, **6**, **7** and **9** as examples on the other side, where the rotational symmetry is violated due to the various heteroatoms in the cyclic π ligands.

Important HF band structure data for **1**–**11** are summarized in Table 1. We have collected the $\varepsilon(k)$ values of the valence and the conduction bands at the centers ($k = 0$, Γ-point) and edges ($k = \pi/c$, X-point) within the first Brillouin zone. $\Delta\varepsilon_{v(c)}$ are the associated band widths of the two dispersion curves. ΔE symbolizes the forbidden band gap of the neutral materials (i.e. absence of injected charge carriers). The types of the gaps and the T_c parameters are given in the last two columns of the table.

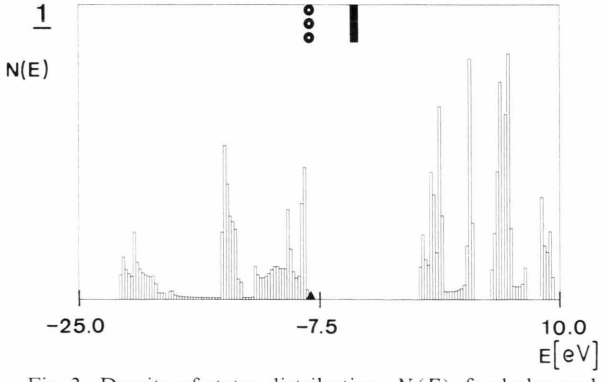

Fig. 3. Density of states distribution, $N(E)$, for holes and particles (i.e. filled and empty Fermi seas) of the cyclopentadienyl Mn polymer **1** in the outer valence region between −25 eV to 10 eV. The $N(E)$ histogram(s) is (are) based on the Hartree-Fock (HF) energy bands derived in the mean-field description. The employed energy grid in the sampling procedures amounts to 0.2 eV. We have adopted individual normalization constants for the representation of the various density of states profiles in the Figs. 3–13. At the bottom of the $N(E)$ plot(s) we have labeled the Fermi level in absence of injected charge carriers by means of a triangle (HF approximation). At the top of the diagram(s) we have indicated the position(s) of the highest occupied microstates with predominant transition metal amplitudes. The circles are associated to HF energies where long- and short-range reorganizations (i.e. electronic correlation and relaxation) are not taken into account. The corresponding quasi-particle (QP) levels are labeled by full bars.

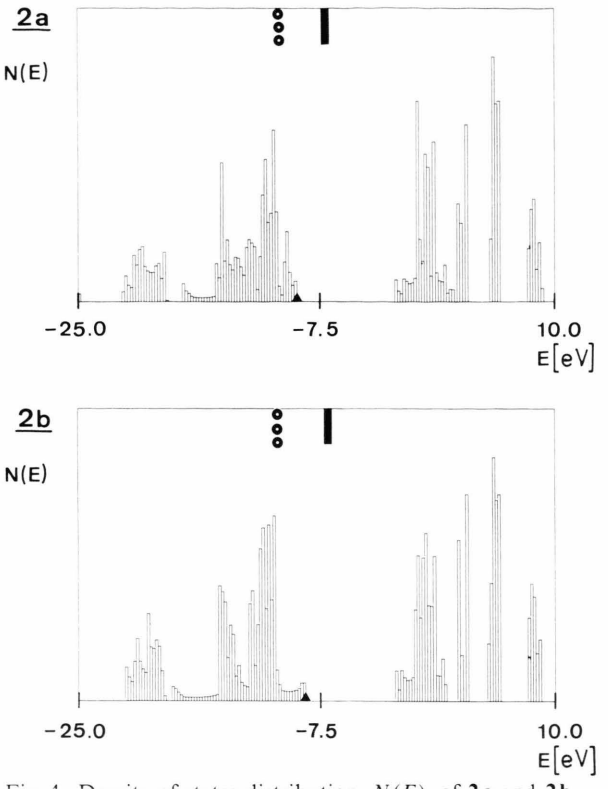

Fig. 4. Density of states distribution, $N(E)$, of **2a** and **2b** in the region between −25 eV to 10 eV; see legend Figure 3. The highest $N(E)$ maxima in the filled one-particle space of both backbones are due to Fe 3d states that belong to narrow dispersion curves.

It is seen that ΔE values up to ca. 8.3 eV are predicted for the 1D materials **1**–**10**, while overlapping bands are only encountered in the Zn system with five B atoms in the cyclic rings; the Fermi energy in this system amounts to −6.57 eV. The energy differences between filled and empty one-particle levels are continuously reduced with an increasing number of B centers in the π moieties; the latter atoms are less electronegative than the carbon sides. In the case of **1** and **11** we have only summarized the HF SCF INDO CO results for the eclipsed chain orientations as the band structure properties of the $\alpha = 0°$ and $\alpha = 180°$ stacks are nearly indistinguishable. This situation is reminiscent of the close correspondence between the D_{5d} and D_{5h} structures of simple metallocene derivatives that are separated by a rotational barrier of only a few kJ/mol [80, 81].

Table 1. Band structure data for the one-dimensional metallocenes **1**–**11** according to semiempirical crystal orbital calculations. The various results have been derived in the fifth neighbour's approximation; ten k-points are considered for the construction of the $\varepsilon(k)$ curves and for the numerical integration of the charge-density-bond-order-matrices. Band energies for the conduction (c) and valence (v) bands are given at the center and the edge of the Brillouin zone, $\varepsilon(0)$ and $\varepsilon(\pi/c)$, respectively. $\Delta\varepsilon_{c(v)}$ symbolizes the associated band width, m_e and m_h are the effective masses for injected electrons or holes. ΔE is the forbidden band gap of the unoxidized materials in the HF approximation. ε_F labels the Fermi energy (conductor) in the case of **11**. The characters of the microstates at the Γ- and X-points are also summarized in the table. The types of the various gaps are given in the last but one column. T_c is the time that corresponds to the propagation of injected charge carriers (holes and electrons) from one unit cell of the 1D stacks to the nearest neighbouring moiety. $\varepsilon(0)$, $\varepsilon(\pi/c)$, $\Delta\varepsilon$ and ΔE are given in eV, T_c in sec. L is an abbreviation for the cyclic π ligands.

1D System	Band	$\varepsilon_c(0)$ $\varepsilon_v(0)$	$\varepsilon_c(\pi/c)$ $\varepsilon_v(\pi/c)$	$\Delta\varepsilon_c$ $\Delta\varepsilon_v$	m_e m_h	ΔE	Character at the Γ-point	Character at the X-point	Type of the gap	T_c (e) T_c (h)
1	c	−0.31	0.60	0.91	7.4	8.27	L (π^*)	L (π^*)	X → Γ	7.28×10^{-16}
	v	−8.19	−8.58	0.58	15.3		Mn $3d_{z^2}$	Mn $3d_{z^2}$		1.14×10^{-15}
2a	c	−0.74	−1.71	2.45	3.6	8.09	L (π^*)	L (π^*), Fe $3d_{xz}$	Γ → X	2.70×10^{-16}
	v	−9.12	−9.38	0.71	12.3		L (π)	L (π)		9.33×10^{-16}
2b	c	−1.78	0.11	1.99	4.4	6.86	L (π^*), Fe $3d_{xz}$	L (π^*)	Γ → Γ	3.33×10^{-16}
	v	−8.55	−10.59	2.40	3.6		L (π)	Fe $3d_{z^2}$		2.76×10^{-16}
3a	c	−0.13	−2.13	2.26	4.5	5.57	L (π^*)	L (π^*), Fe $3d_{yz}$	Γ → X	2.93×10^{-16}
	v	−7.71	−10.25	3.17	3.2		L (π)	Fe $3d_{z^2}$		2.09×10^{-16}
3b	c	−2.02	0.01	2.03	5.0	5.75	L (π^*), Fe $3d_{yz}$	L (π^*)	Γ → Γ	3.26×10^{-16}
	v	−7.78	−10.49	3.03	3.4		L (π)	Fe $3d_{z^2}$		2.19×10^{-16}
4a	c	−0.04	−4.07	4.03	2.1	4.28	L (π^*)	L (π^*), Fe $3d_{yz}$	Γ → X	1.64×10^{-16}
	v	−8.34	−9.98	2.24	3.8		L (π)	L (π)		2.96×10^{-16}
4b	c	−4.19	−0.74	3.36	2.6	3.28	L (π^*), Fe $3d_{yz}$	L (π^*)	Γ → Γ	1.97×10^{-16}
	v	−8.00	−11.10	3.28	2.6		L (π)	L (σ)		2.02×10^{-16}
5a	c	−0.35	−3.75	3.39	2.6	4.90	L (π^*)	L (σ^*), Co $3d_{xz}$	Γ → X	1.95×10^{-16}
	v	−8.65	−9.50	0.87	10.1		L (π)	L (π)		7.61×10^{-16}
5b	c	−1.82	−0.43	1.62	5.4	6.36	L (π^*)	L (π^*)	a)	4.09×10^{-16}
	v	−8.67	−9.59	1.72	5.1		L (σ), Co $3d_{xz}$	L (σ)		3.85×10^{-16}
6a	c	−0.02	−4.87	4.85	1.8	4.85	L (π^*)	L (σ^*), Ni $3d_{yz}$	Γ → X	1.37×10^{-16}
	v	−8.68	−10.04	1.43	6.0		L (π)	L (π)		4.63×10^{-16}
6b	c	−3.65	−1.11	2.58	3.3	5.56	L (σ^*), Ni $3d_{yz}$	L (π^*)	X → Γ	2.57×10^{-16}
	v	−10.32	−9.21	1.11	7.7		L (σ)	L (σ)		5.97×10^{-16}
7a	c	0.69	−5.41	6.09	1.6	1.87	L (σ^*)	L (σ^*), Ni $3d_{xz}$	Γ → X	1.09×10^{-16}
	v	−7.28	−9.48	2.58	3.7		L (π)	L (π)		2.57×10^{-16}
7b	c	−3.91	−1.72	2.33	4.1	4.10	L (π^*)	L (π^*)	b)	2.85×10^{-16}
	v	−9.80	−10.15	2.74	3.5		L (σ), Ni $3d_{xz}$	L (σ)		2.42×10^{-16}
8a	c	−0.63	−4.19	3.55	2.4	4.00	L (π^*)	L (σ^*), Ni $3d_{yz}$	Γ → X	1.87×10^{-16}
	v	−8.19	−9.54	2.73	4.3		L (π), Ni $3d_{xz}$	L (n), Ni $3d_{xz}$		2.43×10^{-16}
8b	c	−4.25	−1.18	3.17	2.7	3.58	L (σ^*), Ni $3d_{yz}$	L (π^*), Ni $3d_{yz}$	X → Γ	2.09×10^{-16}
	v	−9.45	−7.83	2.62	3.3		L (π)	L (π), Ni $3d_{xz}$		2.53×10^{-16}
9a	c	−0.96	−4.13	3.20	2.3	3.24	L (π^*), Ni $3d_{yz}$	L (σ^*), Ni $3d_{yz}$	Γ → X	2.08×10^{-16}
	v	−7.37	−10.33	2.96	2.5		L (π)	L (π)		2.24×10^{-16}
9b	c	−4.16	−1.15	3.01	2.5	2.76	L (σ^*), Ni $3d_{yz}$	L (π^*), Ni $3d_{yz}$	X → Γ	2.21×10^{-16}
	v	−10.02	−6.91	3.11	2.4		L (π), Ni $3d_{xz}$	L (π), Ni $3d_{xz}$		2.14×10^{-16}
10a	c	−2.90	−5.45	2.55	2.7	4.41	L (σ^*)	L (π^*)	Γ → X	2.60×10^{-16}
	v	−9.86	−12.59	3.51	3.7		L (π)	L (σ)		1.89×10^{-16}
10b	c	−4.47	−5.61	1.13	8.5	3.70	L (π^*)	L (σ^*)	c)	5.88×10^{-16}
	v	−13.53	−9.30	4.23	2.3		L (σ)	L (π)		1.57×10^{-16}
11	c*	−2.87	−7.17	4.30	2.2	ε_F =	L (σ^*), Zn $3d_{xz}/3d_{yz}$	L (σ^*), Zn $3d_{xz}/3d_{yz}$		1.54×10^{-16}
	v*	−6.19	−14.91	9.38	1.0	−6.57	L (π)	Zn $3d_{z^2}$		7.08×10^{-17}

* The symbols c and v have been used for the overlapping energy bands in the conducting modification.
a) $(\pi/3\,c) \rightarrow (\pi/4\,c)$. b) $(\pi/3\,c) \rightarrow \Gamma$. c) X → $(\pi/2\,c)$.

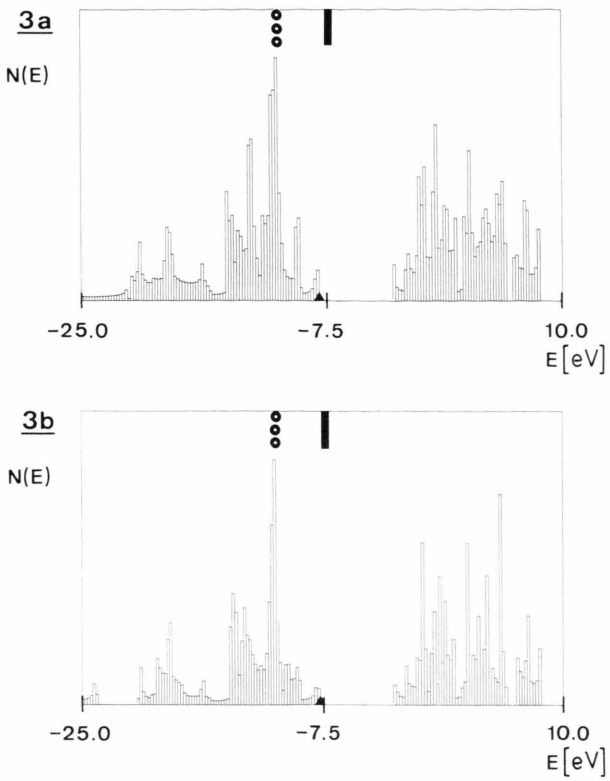

Fig. 5. Density of states distribution, $N(E)$, of **3a** and **3b** in the region between -25 eV to 10 eV; see legend Figure 3. The $N(E)$ maxima in the filled one-particle space once again must be traced back to Fe 3d states in narrow $\varepsilon(k)$ curves. The staggered polymer shows an energy gap in the extreme outer valence region (-23.7 eV to -21.0 eV), while a complex $N(E)$ profile without any gaps is predicted in the $\alpha = 0°$ modification.

On the other side larger differences in the band structure properties are predicted for systems with heteroatoms in the ligand moieties. The magnitudes of the forbidden band gaps and the positions of the top of the valence bands and the bottom of the conduction bands in these strands depend critically on the mutual orientation of the stacking units. The largest changes of ΔE as a function of α amount to ca. 2.2 eV (**7a/7b**); usually the differences are found in an interval between 0.5 to 1.5 eV. Most of the forbidden band gaps in the transition metal stacks are indirect. The results summarized in Table 1 indicate that the shapes of the valence and conduction bands in the eclipsed and staggered chain orientations show often an image–reflected image relation. Strong perturbations of the dispersion curves due to avoided curve crossings on the other side cause violations from these $\varepsilon(k)$ symmetries. Significant mutual repulsions of the dispersion curves in k-space are clearly seen in the $\varepsilon(k)$ representations of **4a/4b**, **6a/6b**, and **7a/7b**, respectively. An avoided $\varepsilon(k)$ crossing between filled and unfilled energy bands leads to an $\varepsilon_v(k)$ maxima at $k = \pi/3c$ in the last example (**7b**).

The calculated band widths for the conduction and valence bands of **1**–**11** span a wide range from ca. 0.6 eV (**1**) to 9.4 eV (**11**). The $\Delta\varepsilon$ parameters are of course enlarged with an increasing number of B atoms in the ligand fragments. This behaviour must be expected as the diffuse 2p functions of the B centers show a stronger overlap with the 3d valence set of the transition metal centers and also a larger ligand-ligand interaction. Such an enlarged mutual coupling in the boron complexes compared to structurally related carbon derivatives has been verified in several theoretical and photoelectron spectroscopic investigations [82, 83]. The majority of

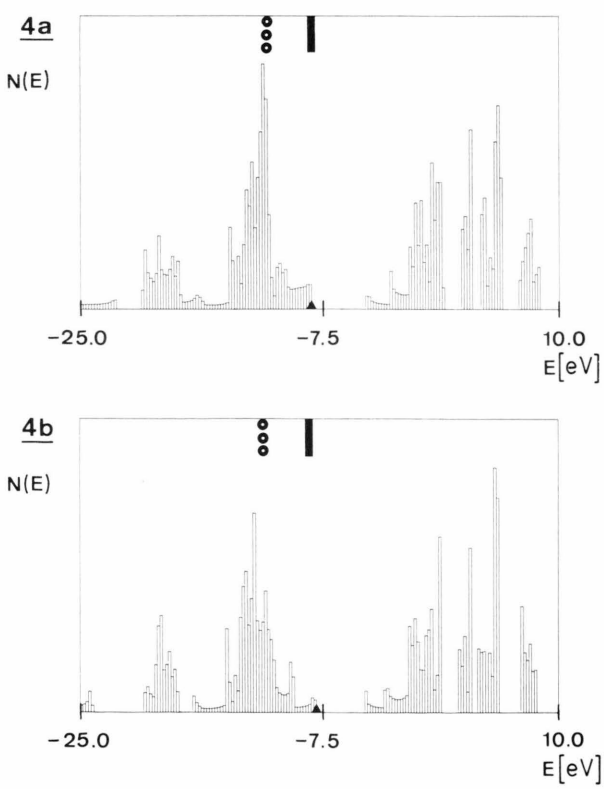

Fig. 6. Density of states distribution, $N(E)$, of **4a** and **4b** in the region between -25 eV to 10 eV; see legend Figure 3.

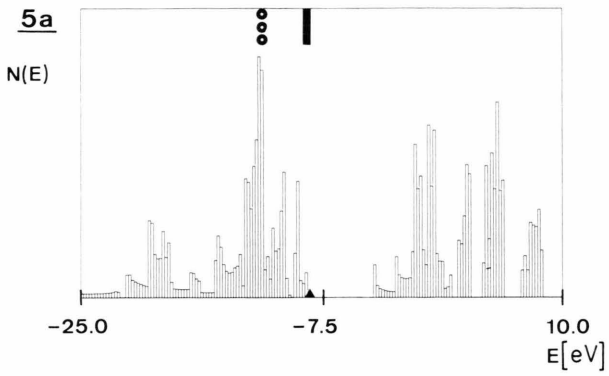

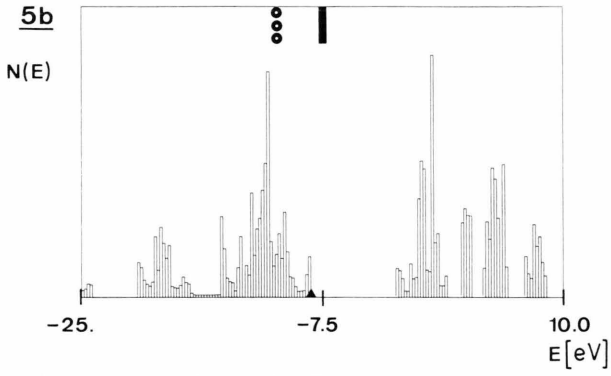

Fig. 7. Density of states distribution, $N(E)$, of **5a** and **5b** in the region between -25 eV to 10 eV; see legend Figure 3. The different transfer channels (injected holes) in the $\alpha = 0°$ backbone (organic metal with band conductivities) and the $\alpha = 180°$ orientation (3d conductor with an activated hopping transfer of charge carriers) is clearly recognized in the two representations (i.e. positions of the full bars on the top of the two $N(E)$ histograms).

the $\Delta\varepsilon_v/\Delta\varepsilon_c$ values is found in an interval between 1.5 and 3.5 eV. The associated effective masses for injected holes and electrons span a range between 1.0 and 15.3; strong deviations from the free electron behaviour are thus predicted for most of the charge carriers. An exception is the B stack **11** where m_h reachs the free electron limit due to a very broad "valence" band. The various T_c parameters differ by an order of ca. 10^2. The largest number is $1.14 \cdot 10^{-15}$ sec, the smallest T_c value amounts to $7.08 \cdot 10^{-17}$ sec. This T_c spectrum indicates the importance of short-range reorganization effects in the studied 1D systems as a result of the long lifetimes of electrons and holes at the various lattice sites. The slowest "hopping rates" exceed fast phonon frequencies in convenient organometallic moieties only by one power.

A detailed inspection of the computational data collected in Table 1 shows that most of the valence bands are of ligand (π or σ) character (HF approximation). Valence states with predominant transition metal amplitudes are only predicted in the Mn and Fe polymers **1**–**3** (exception: **2a**). The valence band of the Mn stack is of $3d_{z^2}$ character at both marginal k-points. The CO properties within a given band are thus conserved as a function of the k-vector. This conservation of the CO amplitudes is

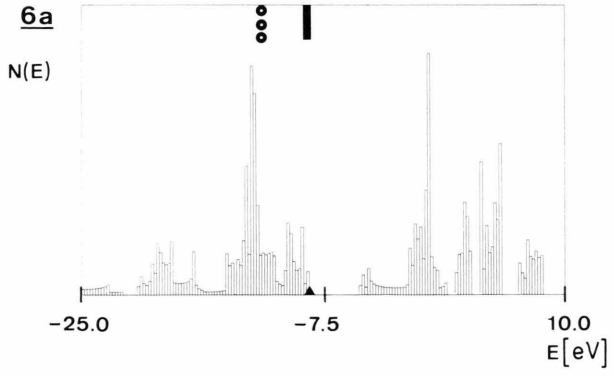

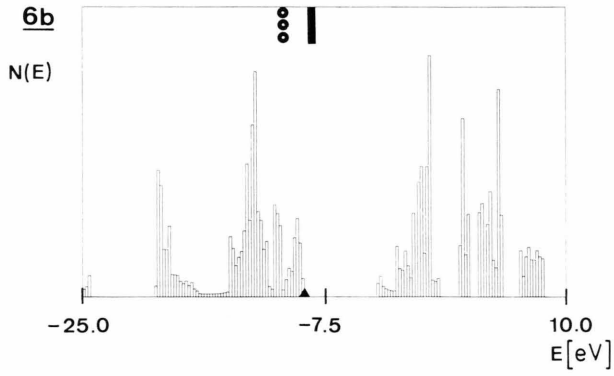

Fig. 8. Density of states distribution, $N(E)$, of **6a** and **6b** in the region between -25 eV to 10 eV; see legend Figure 3. The coalescence between the $N(E)$ maxima in the filled Fermi sea (HF approximation) and the highest occupied metal 3d states encountered in the previous model polymers is violated in the $\alpha = 180°$ stack as a result of the highly populated Ni $3d_{yz}$ states that are involved in a broader dispersion curve. The pronounced $N(E)$ maxima in the lower $N(E)$ histogram (filled one-particle space) must be traced back to Ni $3d_{z^2}$, $3d_{x^2-y^2}$ and $3d_{xy}$ states that belong to narrow $\varepsilon(k)$ curves as a result of their small metal-ligand overlap. The α-dependence of the transfer-channels (injected holes) is clearly visualized in the two diagrams. **6a** belongs to the group of organic metals with conducting ligand states, while the charge carrier pathway in **6b** is prevailingly formed by the Ni 3d spine.

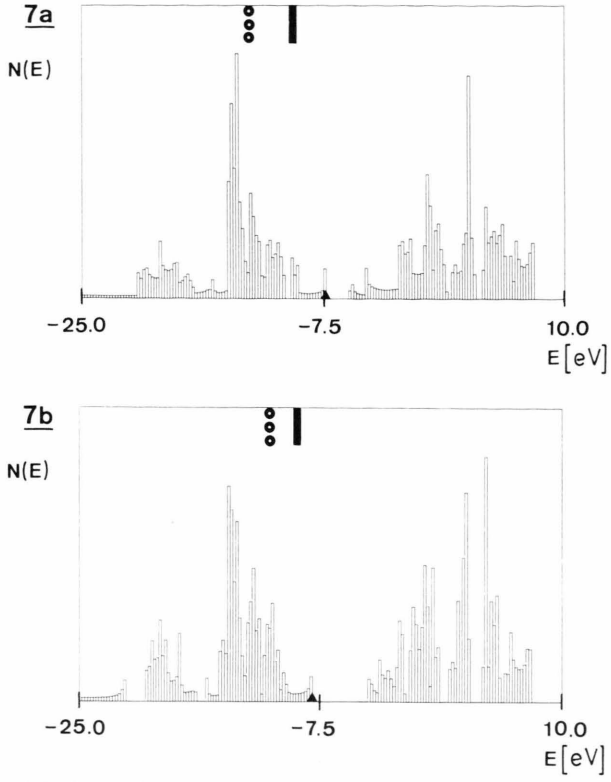

Fig. 9. Density of states distribution, $N(E)$, of **7a** and **7b** in the region between −25 eV to 10 eV; see legend Figure 3. The labels for the highest occupied 3d states in the HF approximation and in the quasi-particle (QP) description show the strong energy dependence of the 3d states on the mutual orientation of the neighbouring building moieties in the 1D solid. The large separations between the $N(E)$ maxima in the occupied Fermi sea (Ni $3d_{z^2}$, $3d_{x^2-y^2}$ and $3d_{xy}$ states) and the HF labels (circles) are the result of highly populated Ni $3d_{yz}$ states that form broader energy bands. The two $N(E)$ histograms show furthermore the significant α-dependence of the forbidden energy gap.

not found in the case of the iron derivatives **2b**, **3a** and **3b**. The states at the bottom of the valence bands are Fe $3d_{z^2}$ functions (X-point), while the microstates at the top of the bands are diffuse ligand orbitals (Γ-point). Pronounced 3d admixtures in the valence bands are furthermore predicted in the electron-rich Ni derivatives **8** and **9**. The geometrical conditions (torsional angle α) favouring or suppressing the efficient population of the Ni $3d_{xz}$ or Ni $3d_{yz}$ orbitals are clearly seen in Table 1 and are therefore not discussed in detail.

Two situations must be discriminated to classify the nature of the filled and unfilled bands in the 1D stacks **1**–**11**: a) Conservation of the character of the microstates as a function of k within a given dispersion curve; b) strong k-dependence of the microstates due to avoided curve crossings in reciprocal k-space. The collected $\varepsilon(k)$ plots in the Figs. 14–19 indicate increasing deviations of the $\varepsilon(k)$ curves from the shapes of "unperturbed tight-binding bands" in 1D materials with reduced spatial symmetries in the stacking units (i.e. **1** and **11** with fivefold axes vs. **2**–**10**, where only a mirror plane in the direction of the longitudinal axis is found within the ML units, $\alpha = 0°$). A reduction in the number of different irreducible representations leads immediately to an enlarged number of crossing regions between the $\varepsilon(k)$ curves in k-space. Various types of k-dependent modifications of microstates can be extracted from Table 1. Typical intraligand changes in the virtual subspace are $\pi^* \rightarrow \sigma^*$ "correlations" or transformations between diffuse pure ligand

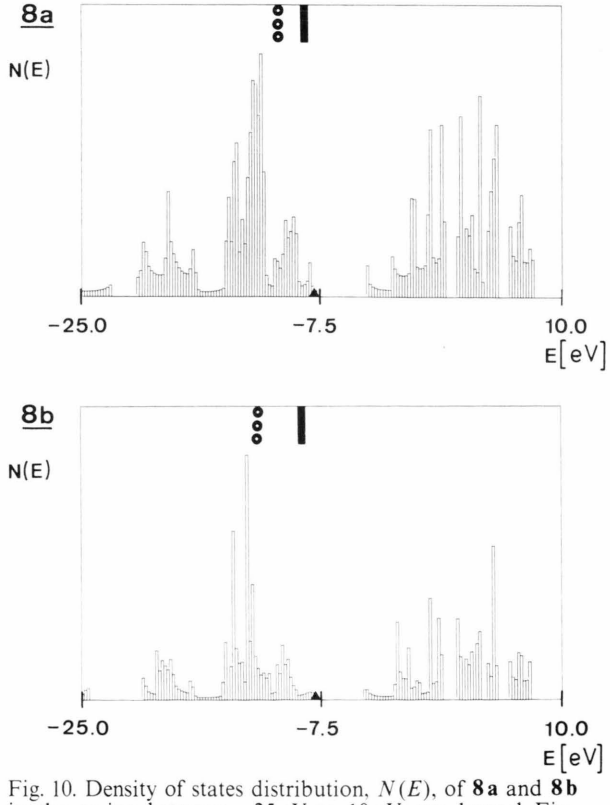

Fig. 10. Density of states distribution, $N(E)$, of **8a** and **8b** in the region between −25 eV to 10 eV; see legend Figure 3. In analogy to the 1D pair **7a**/**7b** once again a strong dependence of the Ni 3d filling scheme on the conformation of the poly-decker is observed. In contrast to **7**, however, highly populated Ni $3d_{yz}$ orbitals are predicted for the eclipsed chain.

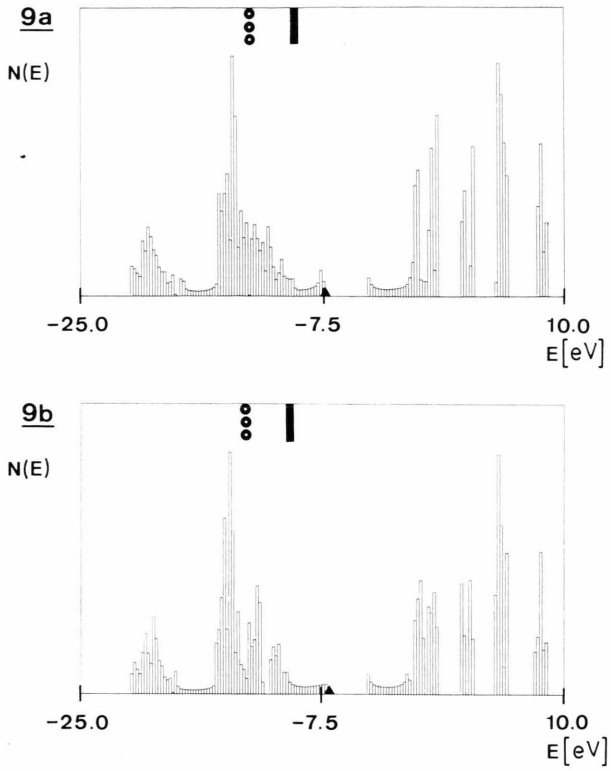

Fig. 11. Density of states distribution, $N(E)$, of **9a** and **9b** in the region between −25 eV to 10 eV; see legend Figure 3.

states (π^*, σ^*) and microstates with comparable metal 3d and ligand admixtures. Intraligand transformations in the filled Fermi sea are once again $\pi \rightarrow \sigma(n)$ processes that conserve roughly the localization properties of the CO wave functions (i.e. magnitude of the on-site electron-electron integrals). The intracell localization of the microstates, however, depends critically on the value of the k-vector in those dispersion curves, where ligand (metal) amplitudes are transferred into metal (ligand) states. The necessary modifications of the HF results in Table 1 (i.e. relative sequence of the metal and ligand states in the quasi-particle picture) will be discussed below.

The band energies as derived in the HF approximation for the "transition metal 3d states" (occupied one-particle space) of some 1D materials are summarized in Table 2 (**1**, **6a/6b**, **9a/9b**). Only three occupied bands with large Mn 3d amplitudes ($3d_{z^2}$ band with a_1 symmetry, degenerate $3d_{x^2-y^2}/3d_{xy}$ band with e_2 symmetry) are predicted in the Mn derivative **1**; these bands are found on top of the highest occupied ligand states. The Ni 3d functions in the heterosystems **6** and **9** on the other side are several eV below the high-lying ligand π and σ functions. A comparable switch in the sequence of the 3d and ligand states as a function of the 3d atom has been detected in semiempirical MO calculations on simple closed shell metallocenes [84]. Ab initio studies on the HF ground states of 3d (Fe, Ni) ligand π complexes lead also to a MO sequence, where the highest ligand functions are on top of the 3d set [85, 86]. The simple three below two splitting pattern in the Mn system **1** (i.e. occupied $3d_{z^2}$, $3d_{x^2-y^2}/3d_{xy}$ states, virtual $3d_{xz}/3d_{yz}$ functions) is perturbed in the heterosystems **6** and **9** with the reduced lattice symmetries or the enlarged number of valence electrons (**9**). In **6a** strongly atomic-like $3d_{xz}$ and $3d_{yz}$ states are predicted at the center of the Brillouin zone; they are transferred into microstates with predominant ligand admixtures at

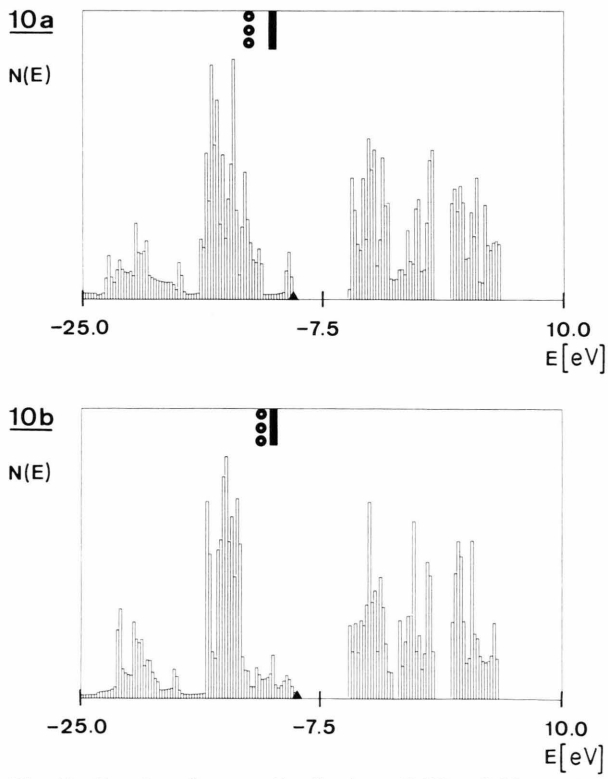

Fig. 12. Density of states distribution, $N(E)$, of **10a** and **10b** in the region between −25 eV to 10 eV; see legend Figure 3.

Table 2. Representative collection of some band energies in the 1D metallocene series (**1**, **6a**, **6b**, **9a** and **9b**, respectively) at the center ($\varepsilon(0)$) and edge ($\varepsilon(\pi/c)$) of the Brillouin zone for those dispersion curves that are characterized due to significant metal 3d amplitudes at (one of) the marginal k-points Γ and X. We have summarized the numbers of the $\varepsilon(k)$ curves, the HF energies and the transition metal admixtures to the crystal orbital wave functions. Different band labels at the center and the edge of the zone indicate that the characters of the (3d) microstates are not conserved as a function of the wave vector k. The numbering scheme of the dispersion curves is associated to the configuration of the valence electrons.

1D system	Type of the 3d states	Band no. Γ	3d admixtures Γ	$\varepsilon(0)$ (eV)	Band no. X	3d admixtures X	$\varepsilon(\pi/c)$ (eV)
1	Mn $3d_{x^2-y^2}/3d_{xy}$	15/16	92.6	−8.46	15/16	75.7	−9.36
	Mn $3d_{z^2}$	14	91.8	−8.54	14	97.2	−8.19
6a	Ni $3d_{yz}$	12	81.9	−12.29	12	37.0	−12.00
	Ni $3d_{z^2}$	11	92.1	−12.62	11	98.6	−11.96
	Ni $3d_{x^2-y^2}$	10	91.3	−12.79	10	94.6	−8.98
	Ni $3d_{xz}$	9	69.0	−13.04	14	39.9	−10.68
	Ni $3d_{xy}$	8	72.7	−13.25	8	96.6	−8.94
6b	Ni $3d_{xz}$	16	36.1	−9.95	11	84.4	−12.42
	Ni $3d_{x^2-y^2}$	12	83.1	−12.51	12	96.3	−12.07
	Ni $3d_{z^2}$	11	90.5	−12.53	13	99.3	−11.88
	Ni $3d_{yz}$	10	56.6	−12.64	14	75.5	−10.59
	Ni $3d_{xy}$	9	61.1	−13.17	9	96.4	−12.08
9a	Ni $3d_{yz}$	14	54.3	−12.45	14	14.1	−10.92
	Ni $3d_{z^2}$	12	93.1	−13.64	13	93.7	−12.80
	Ni $3d_{xy}$	11	74.3	−13.81	11	98.3	−13.19
	Ni $3d_{x^2-y^2}$	10	89.4	−13.85	10	98.2	−13.19
	Ni $3d_{xz}$	8	83.9	−14.85	8	55.2	−13.92
9b	Ni $3d_{yz}$	15	16.0	−11.94	15	54.1	−11.61
	Ni $3d_{z^2}$	12	92.7	−13.87	13	93.6	−13.05
	Ni $3d_{x^2-y^2}$	11	70.2	−14.03	11	98.7	−13.44
	Ni $3d_{xy}$	10	64.6	−14.04	10	98.3	−13.46
	Ni $3d_{xz}$	7	64.2	−15.04	8	90.6	−14.01

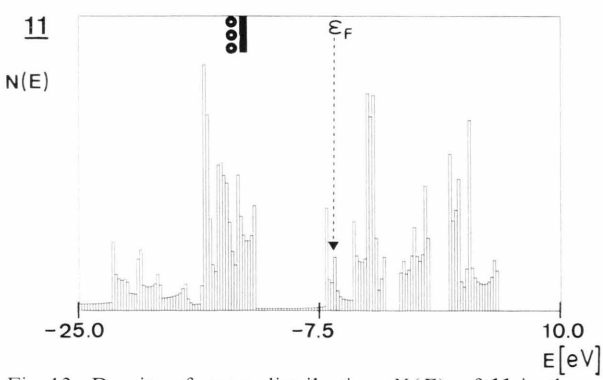

Fig. 13. Density of states distribution, $N(E)$, of **11** in the region between −25 eV to 10 eV; see legend Figure 3. The two $N(E)$ maxima embedding the Fermi energy ε_F (= −6.57 eV) are due to the Γ- and X-singularities of the overlapping energy bands that lead to the metallic state in the Zn backbone (see also Figure 19).

$k = \pi/c$. Almost the opposite pattern is observed in the staggered arrangement **6b**. The $3d_{xz}$ and $3d_{yz}$ AO populations are still enhanced in **9** as a result of the two additional electrons. These examples show explicitly the strengthened metal-ligand coupling in the B complexes, an interaction pattern that allows the reduction of the forbidden energy gap. The conduction bands are shifted downwards and are also broadened due to the modified interactions within the B-substituted 1D stacks.

The band energies of the "3d dispersion curves" of **1**, **6** and **9** at the Γ- and X-points show that the characters of the CO wave functions are often not conserved in k-space. Metal-ligand transformations already have been mentioned. The low spatial symmetries of the heterostacks allow furthermore "correlations" between different types of 3d functions (e.g. Ni $3d_{z^2}(\Gamma) \rightarrow$ Ni $3d_{xz}$(X) in **6b**). The symmetry reduction in the 1D lattice and the influence of the heteroatoms violates in any case the simple one-electron (orbital) picture that is found in metallocene complexes; here three nonbonding 3d functions with small or even negligible 3d admixtures are strictly discriminated from the diffuse ligand orbitals [84, 85]. In the low-dimensional materials also CO wave functions are encountered, that show comparable metal and ligand admixtures.

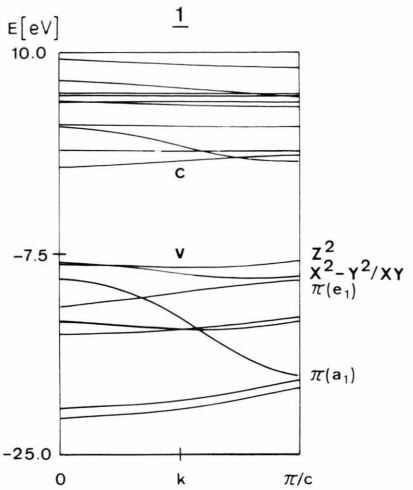

Fig. 14. Hartree-Fock (HF) energy bands of the Mn polydecker **1** in the interval between −25 eV to 10 eV. The valence band of the undoped polymer is symbolized by v, the conduction band by c. The character of some characteristic HF bands is labeled at the edge of the Brillouin zone. z^2 is the abbreviation for the Mn $3d_{z^2}$ dispersion; x^2-y^2/xy is associated to the degenerate Mn $3d_{x^2-y^2}/3d_{xy}$ band, $\pi(e_1)$ to the degenerate ligand (= cyclopentadienyl) π band of e_1 symmetry and $\pi(a_1)$ to the symmetric ligand π band.

In Table 3 we have collected the energies of the highest occupied transition metal states in the quasi-particle approximation. The calculated shifts amount to 3.0−3.3 eV in the Mn, Fe and Co stacks. They are reduced to 1.6−0.5 eV in the Cu and Zn sandwich compounds. For the diffuse ligand states self-energy corrections of ca. 0.3−0.5 eV can be assumed in the outer valence region [72]. It is seen that the 3d states in **1**, **2** and **3** are well separated from the ligand bands if correlation and relaxation effects are taken into account. Injected holes belong to the transition metal spines and thus should give raise to a hopping type conductivity. Most of the Co and Ni model polymers belong to the group of the organic metals in the case of partial oxidation. The conductive pathways in the Cu and Zn systems are exclusively determined by states of the heteroligands.

Our model calculations predict in some of the 1D stacks near degeneracies between conduction processes in the ligand framework and hopping conductivities in the 3d manifold (injected holes). Such doubly mixed valence states with oxidation processes that are both ligand and metal centered, e.g.,

Table 3. Collection of the highest occupied microstates in the 1D metallocene series **1**–**11** with predominant transition metal 3d amplitudes. The types of the 3d states are summarized in the second column, their admixtures to the CO wave functions are given in column 3. $\varepsilon(k)$ is the one-electron energy derived in the Hartree-Fock approximation of the semiempirical crystal orbital formalism. $\varepsilon_{QP}(k)$ symbolizes the associated quasi-particle energy based on HF dispersions that have been corrected by means of long-range and short-range electronic correlations (and relaxations). 1D stacks with injected holes are discriminated into organic metals (OM) and transition metal systems (TM). The conductive pathway is formed by ligand states in the first case and by the 3d spine in the latter materials. The conduction processes thus can be classified into band conductivities (B) and into hopping transfer processes (H).

1D system	Type of the 3d states	3d admixtures (%)	$\varepsilon(k)$ (eV)	$\varepsilon_{QP}(k)$ (eV)	k value	Conducting modification	Conduction process
1	Mn $3d_{z^2}$	97.2	−8.19	−5.19	Γ	TM	H
2a	Fe $3d_{z^2}$	88.4	−10.44	−6.89	X	TM	H
2b	Fe $3d_{z^2}$	85.0	−10.50	−6.85	X	TM	H
3a	Fe $3d_{x^2-y^2}$	85.2	−10.60	−7.05	Γ	TM	H
3b	Fe $3d_{xy}$	92.3	−10.83	−7.28	X	OM/TM	B/H
4a	Co $3d_{x^2-y^2}$	93.1	−11.52	−8.22	X	OM	B
4b	Co $3d_{z^2}$	99.6	−11.71	−8.41	X	OM	B
5a	Co $3d_{z^2}$	85.4	−11.98	−8.68	Γ	OM	B
5b	Co $3d_{z^2}$	98.6	−10.90	−7.60	X	TM	H
6a	Ni $3d_{z^2}$	99.3	−11.96	−8.76	X	OM	B
6b	Ni $3d_{yz}$	75.5	−10.59	−8.59	X	TM	H
7a	Ni $3d_{z^2}$	99.7	−12.96	−9.76	X	OM	B
7b	Ni $3d_{yz}$	68.5	−11.29	−9.29	X	OM	B
8a	Ni $3d_{yz}$	76.8	−10.89	−8.89	Γ	OM	B
8b	Ni $3d_{z^2}$	99.6	−12.16	−8.96	X	OM	B
9a	Ni $3d_{z^2}$	93.7	−12.80	−9.60	X	OM	B
9b	Ni $3d_{z^2}$	93.6	−13.05	−9.85	X	OM	B
10a	Cu $3d_{yz}$	74.1	−12.85	−11.15	Γ	OM	B
10b	Cu $3d_{yz}$	54.7	−11.92	−11.02	Γ	OM	B
11	Zn $3d_{xz}/3d_{yz}$	57.3	−13.98	−13.48	X	OM	B

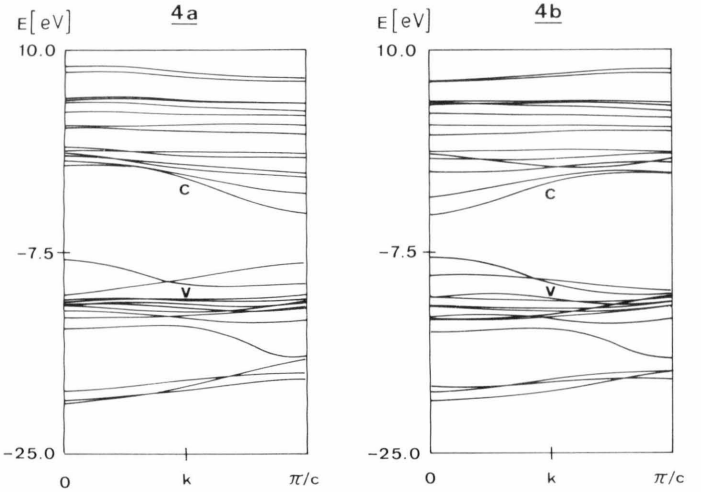

Fig. 15. Hartree-Fock (HF) energy bands of the two Co poly-decker sandwiches **4a** and **4b** in the interval between − 25 eV to 10 eV. The valence band of the unoxidized backbone is symbolized by v, the conduction band by c.

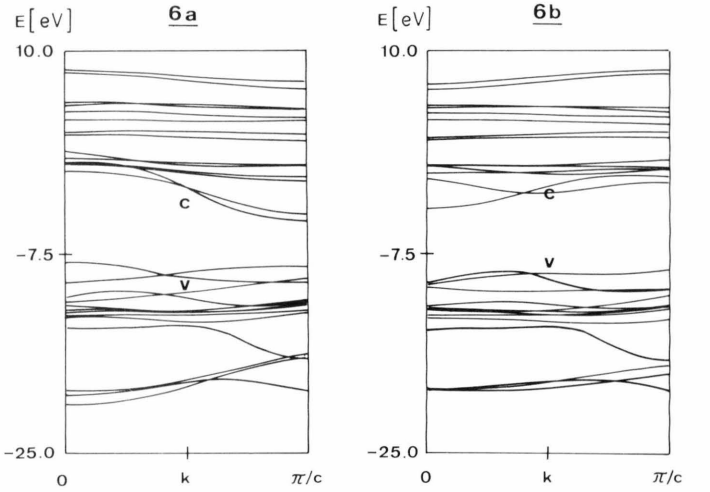

Fig. 16. Hartree-Fock (HF) energy bands of the two Ni strands **6a** and **6b** in the interval between − 25 eV to 10 eV; see legend Figure 15.

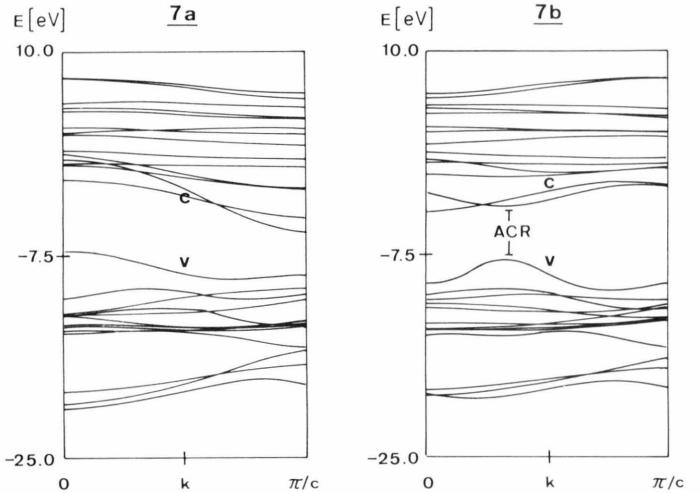

Fig. 17. Hartree-Fock (HF) energy bands of the two Ni backbones **7a** and **7b** in the interval between − 25 eV to 10 eV; see legend Figure 15. In the case of the $\alpha = 180°$ material we have displayed the $\varepsilon(k)$ region where an avoided crossing between the filled and empty Fermi seas is encountered (ACR).

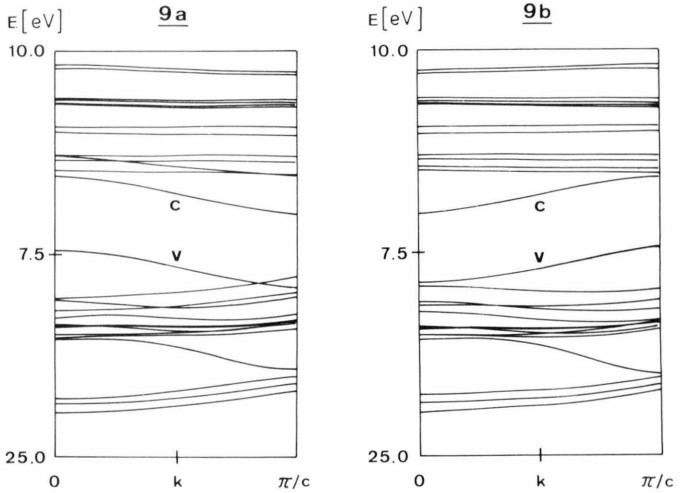

Fig. 18. Hartree-Fock (HF) energy bands of the two Ni chains **9a** and **9b** in the interval between − 25 eV to 10 eV; see legend Figure 15.

Table 4. Energy differences ΔE_{TOT}^{HF} between the eclipsed (**a**) and staggered (**b**) conformations of the 1D metallocenes **1**–**11** according to semiempirical INDO CO calculations. ΔE_{TOT}^{HF} has been derived in the fifth nearest neighbour's approximation; ten k-points have been employed in the computational approaches. $\Delta E_{TOT}^{HF} = E_{TOT}^{HF}(\text{staggered}) - E_{TOT}^{HF}$ (eclipsed). ΔE_{TOT}^{HF} is given in kJ.

	1	**2**	**3**	**4**	**5**	**6**	**7**	**8**	**9**	**10**	**11**
ΔE_{TOT}^{HF}	12.6	109.8	89.9	112.1	88.5	60.5	28.2	0.8	57.6	68.5	2.6

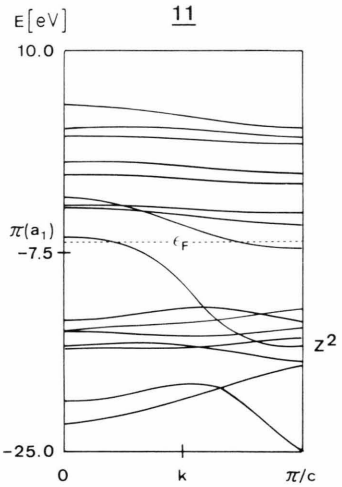

Fig. 19. Hartree-Fock (HF) energy bands of the pentaborolenyl Zn poly-decker **11** in the interval between −25 eV to 10 eV. The Fermi energy ε_F (= −6.57 eV) is labeled in the $\varepsilon(k)$ plot. The character of the CO microstates of the "valence band" (see footnote Table 1) of **11** is indicated at the Γ-point ($\pi(a_1)$) and at the marginal X-point (z^2 = Zn $3d_{z^2}$ states).

have been discussed in conducting tetrabenzporphyrinato nickel(II) stacks [87]. In the staggered conformation of **3** nearly degenerate quasi-particle energies (Fermi levels) for Fe 3d and ligand π states are predicted. The nature of the transfer channels in **5** or **6** depends on the stacking pattern of the 1D materials. The strong upwards shifts of the Co $3d_{z^2}$ (**5**) or Ni $3d_{yz}$ (**6**) levels in the $\alpha = 180°$ orientation leads to a transition from an organic metal ($\alpha = 0°$) to a conducting 3d spine ($\alpha = 180°$) (injected holes).

The energy differences between the eclipsed and staggered polymer conformations of **1**–**11** are summarized in Table 4. Of course only small torsional barriers are found in the highly symmetric transition metal derivatives **1** and **11**. The heteroatoms cause significant energetic separations between the different conformations in the 1D stack. One of the largest ΔE_{TOT}^{HF} figures is found in the pair **2a**/**2b** where the variation of the BB distance vector between adjacent π ligands is largest; a high barrier is also encountered in the diborolene stack **4a**/**4b**. The torsional profile of **4** is displayed in Figure 20. We have shown the relative HF energies ΔE_{TOT}^{HF} as a function of α (E_{TOT}^{HF}(eclipsed) = 0) and the variation of the intracell (E_{INTRA}) and intercell (E_S) energies. The eclipsed conformation corresponds to a sharp minimum. The ascend ΔE_{TOT}^{HF} curve for small libration amplitudes must be traced back to modifications of the intracell energies while the influence of the intercell coupling is strengthened with increasing $\Delta\alpha$ values. The shapes of the various curves indicate that the mutual torsions between the

Table 5. Fragmentation of the total intercell energies of the 1D metallocenes **2a** and **2b** as well as **5a** and **5b**, respectively, into resonance (E_{RES}), exchange (E_{EX}) and classical electrostatic (E_{COU}: Coulomb energy, i.e. sum of electron-electron repulsion, electron-core attraction and core-core repulsion) interaction terms between the reference cell ($j = 0$) and the first ($j = 1$), second ($j = 2$), etc. nearest neighbouring moieties. $E_S = E_{RES} + E_{EX} + E_{COU}$. All values are given in eV.

1D System	j	E_{RES}	E_{EX}	E_{COU}	E_S
2a	1	−21.0722	−4.4356	−1.4475	−27.2553
	2	−0.2028	−0.1328	−0.0894	−0.4250
	3	0.0007	−0.0678	−0.0243	−0.0928
	4	–	−0.0515	−0.0107	−0.0622
	5	–	−0.0414	−0.0054	−0.0468
	1–5	−21.2743	−5.0291	−1.5773	−27.9650
2b	1	−19.9674	−4.5070	−1.5712	−26.0456
	2	−0.1889	−0.1560	−0.0984	−0.4433
	3	0.0008	−0.0657	−0.0347	−0.0995
	4	–	−0.0516	−0.0117	−0.0633
	5	–	−0.0410	−0.0074	−0.0484
	1–5	−20.1555	−4.8213	−1.7234	−26.7002
5a	1	−19.9927	−4.5148	−1.4538	−25.9612
	2	−0.1100	−0.1911	−0.1714	−0.4725
	3	0.0005	−0.0697	−0.0512	−0.1205
	4	–	−0.0525	−0.0215	−0.0740
	5	–	−0.0420	−0.0110	−0.0530
	1–5	−20.1022	−4.8701	−1.7089	−26.6812
5b	1	−19.2133	−3.7569	−1.2683	−24.2386
	2	−0.0777	−0.1855	−0.1329	−0.3961
	3	−0.0009	−0.0707	−0.0435	−0.1133
	4	–	−0.0513	−0.0165	−0.0678
	5	–	−0.0412	−0.0094	−0.0506
	1–5	−19.2919	−4.1056	−1.4706	−24.8681

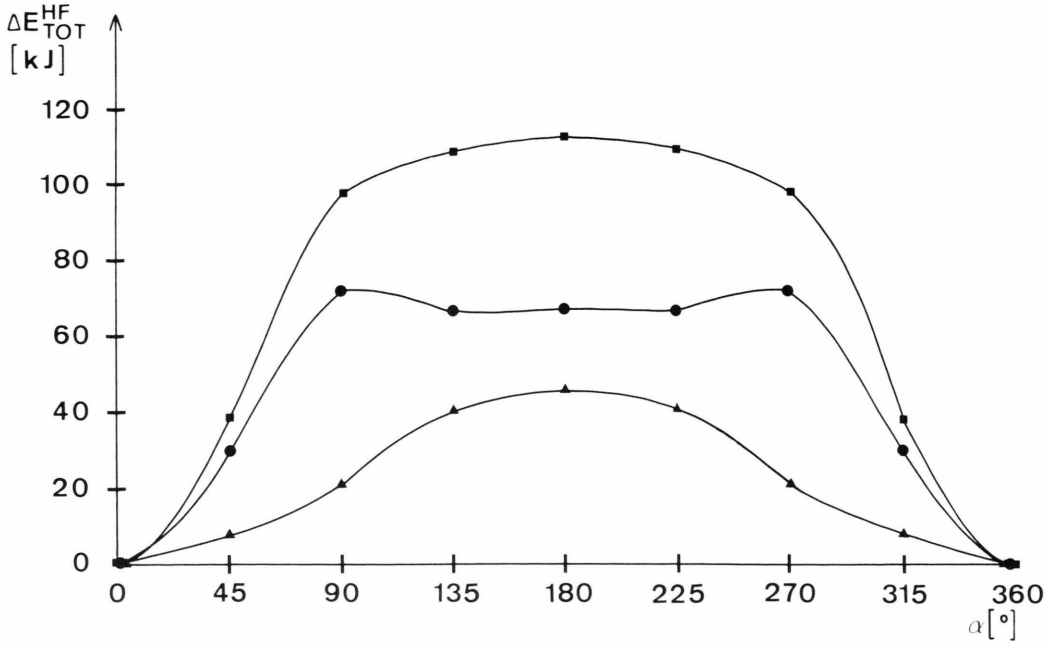

Fig. 20. Rotational barrier ΔE_{TOT}^{HF} of the 1.3-diborolenyl cobalt polymer **4** according to the semiempirical INDO crystal orbital formalism. The net curve ΔE_{TOT}^{HF} is labeled by squares (upper profile). The curve in the middle corresponds to the α-dependent changes of the intercell energies ΔE_S (circles), while the lower one is the modification of the intracell potential ΔE_{INTRA} (triangles). The eclipsed chain conformation ($\alpha = 0°$) has been used as internal standard (ΔE_{TOT}^{HF} ($\alpha = 0$) = 0, ΔE_S ($\alpha = 0$) = 0 and ΔE_{INTRA} ($\alpha = 0$) = 0, respectively).

stacking units are both influenced via electronic rearrangement processes within the unit cells as well as via ligand-ligand interactions of the intercell type. The intracell energies are nearly constant in the interval $90° \leqq \alpha \leqq 180°$ where the rotation is hindered due to the decreasing interaction between the stacking units. The α-dependent variations of the band energies in the metal 3d regimes (see Tables 1 and 3) have obviously their electronic origin in these intracell and intercell rearrangement processes.

To understand the driving forces for the pronounced energy barriers in **2**–**10** (exceptions: **1**, **8** and **11**) we have decomposed the intercell energies E_S of **2a**/**2b** and **5a**/**5b** into the aforementioned resonance, exchange and Coulomb elements E_{RES}, E_{EX} and E_{COU}, respectively (Table 5). The analysis is extremely simple in the Fe system **2**. The difference between the staggered and the eclipsed structure is almost exclusively determined by the covalent resonance energy between nearest neighbours; all other intercell contributions are smaller than 15%. The numerical values of the individual two-center elements show immediately that the E_{RES} variation can be traced back to two coupling elements, i.e. the BB and BFe couples between adjacent building blocks. The diffuse B orbitals (in comparison to C) allow both an efficient direct covalent overlap between the B-over-B stacked heteroatoms and enhance the metal-ligand interaction in the eclipsed conformation. The E_{RES}^{BB} terms exceed E_{RES}^{CC} (interligand parameters) by a factor of ca. 4. The covalent (BB and BFe) interaction is dramatically weakened in the 180° arrangement. This interpretation is obviously in line with the increasing $\Delta\varepsilon$ parameters in the boron-substituted polymers. The energy fragmentation for the Co systems **5a** and **5b** is of larger complexity. The α-dependent variation of the BB vectors is smaller than in the Fe stack **2**. Thus also the width of the E_{RES} elements is reduced in the Co derivatives. The torsional profile is determined in a like manner by the covalent resonance energies and by the exchange parameters E_{EX} (only nearest neighbour's coupling); the modification of the classical electrostatic potential is small in comparison to E_{RES} and E_{EX}. It is

once again the direct BB coupling that leads to the α-dependent differences in the interaction energies. An exception in the series **2**–**10** is the heteroderivative **8**; the stabilizing B-over-B arrangement in an eclipsed stack is reduced by means of the repulsive SS potential that favours the staggered conformation. Both factors (BB and SS interactions) largely compensate each other and therefore only a negligibly small energy difference between the two extreme orientations is predicted. The ΔE_{TOT}^{HF} parameters summarized in Table 4 are encountered in an energetic interval where modifications of the equilibrium geometries (i.e. value of α at the energy minimum) are still possible due to bulky substituents in the organic π ligands [88].

To summarize: Band structure calculations on the mean-field level as well as quasi-particle corrections of the HF bands for the 1D polymers **1**–**11** have shown that only **11** is an intrinsic conductor. The 1D stacks **1**–**10** require injected charge carriers (holes or electrons) to achieve partially filled energy levels. The types of the transfer channels depend critically on the stoichiometry of the organometallic materials and on the mutual orientation of the stacking units. A concise discussion of the electronic structure of the various model stacks will be given in the next section.

4. Discussion

The forbidden band gap in the undoped cyclopentadienyl manganese derivative **1** amounts to 8.27 eV; the gap is indirect ($\Gamma \rightarrow X$). The acceptor levels of **1** are found at rather high energies. The injection of electrons thus should be ruled out in synthetic routes to conducting modifications of **1**. Partial oxidation would lead to injected holes that propagate within the Mn 3d spine via a diffusive hopping motion. Details of these hole-state properties will be discussed in a subsequent contribution [89]. The dispersion curves of **1** (Fig. 14) show the absence of extensive crossing regions in k-space. The extremely broad energy band between -18.20 eV to -9.81 eV ($\Delta\varepsilon = 8.4$ eV) in the $\varepsilon(k)$ plot is associated to ligand π states of a_1 symmetry. The effective mass parameter for injected holes ($m_h = 1.04$) associated to this dispersion curve is very close to the free electron value.

The formation of broad ligand π bands is prevented in the 1D stacks **2**–**10**; the reduced lattice

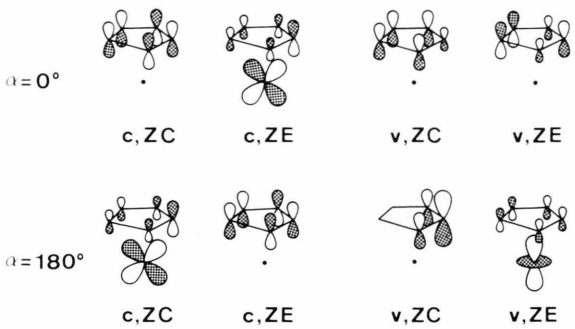

Fig. 21. Schematic representation of the crystal orbital amplitudes of the conduction (c) and valence (v) bands at the center of the Brillouin zone (ZC, $k = 0$) and at the zone edge (ZE, $k = \pi/c$) in the Fe derivatives **2a** and **2b** (top and bottom of the figure).

symmetry is the topological origin for pronounced modifications of the CO wave functions as a function of the k-vector. This behaviour is demonstrated in Fig. 21, where the CO amplitudes of the conduction and valence bands of **2a** and **2b** are displayed at the center and the edge of the Brillouin zone. It is obvious that such "correlations" between different types of CO microstates are forbidden in the 1D stacks with the fivefold rotation axes. The symmetry relations between the CO amplitudes at the two marginal k-points are clearly seen in the conduction bands of **2a** and **2b**. This behaviour is not found in the occupied subspace (valence band); the localization properties of the CO's are completely different in **2a** on one side and **2b** on the other side. The band gap in the 0° stack is indirect ($\Gamma \rightarrow X$) while a direct gap at the center of the Brillouin zone is predicted in the 180° arrangement. The largest $\Delta\varepsilon$ parameters in the outer valence region are reduced to ca. 2.5 eV. The positions of the conduction and valence bands in **2a** and **2b** (energy criterion) suggest once again the injection of holes in aspired conducting modifications of the 1D metallocene. The $\varepsilon(k)$ profiles and the $N(E)$ distributions of **3a** and **3b** are closely related to the one-electron properties of **2a** and **2b** and are therefore not discussed in detail. The additional B atom per unit cell however leads to a reduction of the forbidden band gap (ca. 1.5–2.0 eV).

A relatively small direct gap at the center of the Brillouin zone is predicted in the staggered ($\alpha = 180°$) chain conformation of the 1,3-diborolene derivative **4b**. The shape of the valence band is roughly conserved as a function of α. The disper-

sions of the conduction bands show the aforementioned mirror symmetry in the pair **4a** and **4b**. There exists an 1:1 correspondence between the CO amplitudes in the conduction bands of the eclipsed and staggered chains. The repulsion between the highest filled and lowest unfilled dispersion curves in the staggered backbone **4b** suggests the existence of a finite band gap even under high-pressure conditions. The $\varepsilon(k)$ profile in the 0° system on the other hand should allow an insulator-to-metal transition under pressure. Test calculations as a function of the unit cell dimension have shown that c-reductions of 10–15% are necessary to force an insulator-to-metal transition. In Fig. 15 it is furthermore displayed that the indirect gap ($\Gamma \rightarrow$ X) in the eclipsed stack is nearly degenerate with a direct one (energy difference: 0.08 eV) at the edge of the Brillouin zone leading to the coexistence of photoconducting properties, that would require phonon absorptions to conserve the crystal momentum, and excitations that are not coupled to lattice vibrations. The microstates at the marginal k-points in the valence band of **4a** are of ligand π character with vanishing transition metal admixtures. The valence band of **4b**, however, shows ligand σ states at the X-point. This variation of the crystal orbitals as a function of the k-vector is still enhanced in the 1.2-diborolene system **5a/5b**, where the BB bonds cause strongly destabilized ligand σ states in the outer energy region.

The valence band in the eclipsed chain is of ligand π character both at the Γ- and the X-point. The highest filled band in the staggered backbone is a σ-type function with Co $3d_{xz}$ admixtures at the center of the Brillouin zone; the transition metal amplitudes are reduced with increasing values of the k-vector. The smallest forbidden gap ΔE in **5b** is predicted at $(\pi/3c)$. The close contact between the filled and unfilled dispersions once again must be traced back to avoided curve crossings in k-space. The k-dependence of the microstates of **5** is displayed in Fig. 22; we have shown the CO wave functions of the valence band at the k-points Γ and X as well as the amplitudes of the conduction band at the center of the Brillouin zone ($\alpha = 0°$ polymer). The acceptor levels in the two diborolene Co stacks **4** and **5** are significantly lowered in comparison to **1**, **2** or **3** and are, e.g., comparable with the $\varepsilon(k)$ spectrum of the lowest unfilled band in tetrathiosquarato nickel(II). This band is occupied by 0.08 electrons in

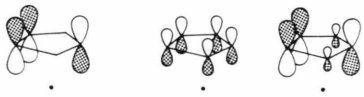

Fig. 22. Schematic representation of the crystal orbital amplitudes of the conduction (c) and valence (v) bands at the center of the Brillouin zone (ZC) and the zone edge (ZE) in the 1.2-diborolenyl Co poly-decker **5a** (eclipsed 0° conformation). In the case of the conduction band only the CO amplitudes at the Γ-point are displayed in this figure.

the conducting state of the low-dimensional material [7, 30]. Thus it can be assumed that the injection of electrons via strong donors (e.g., alkaline atoms, K, Na) should be possible in 1D materials as **4** or **5** with their electropositive heteroatoms. The depression of the virtual Fermi sea is still enhanced in the Ni polymers **6** and **7** containing three B centers per fivemembered ring.

A near degeneracy between a direct gap at the edge of the Brillouin zone as well as an indirect gap ($\Gamma \rightarrow$ X) is predicted in the 0° modification of **6** (see Figure 16). The valence band in the 0° stack is of ligand π character at both marginal k-points. The broad conduction band is characterized due to ligand π^* states at the zone center while the X-states are σ^* linear combinations which are strongly coupled with Co $3d_{xz}$ functions. This efficient metal ($3d_{xz}$ or $3d_{yz}$)-ligand (B AO's) overlap allows the formation of the broad conduction bands in some of the presented 1D poly-decker sandwiches. The reduced π overlap in the 180° conformation is responsible for a switch in the sequence of the highest filled bands in the eclipsed strand on one side and the staggered backbone on the other; the microstates in the valence band of **6b** are ligand σ functions that are prevailingly localized in the BBB moieties. **6a** is one of the sparse examples in the series of the heteroderivatives, where the CO amplitudes within the 3d manifold are conserved as a function of k (see Table 2). The localization properties of the $3d_{z^2}$, $3d_{x^2-y^2}$ and $3d_{xy}$ bands are nearly constant within the three dispersion curves.

The energetic width between the filled and unfilled bands is reduced if the three B atoms in the cyclic π ligand are separated by carbon centers (**7a/7b**). The ΔE number in **7a** amounts to only 1.87 eV, but is enlarged to 4.10 eV in the staggered arrangement. The 1.87 eV gap is indirect ($\Gamma \rightarrow$ X)

offering the possibility of an insulator-to-metal transition under pressure. The $\varepsilon(k)$ profiles of **7a** and **7b** show a large number of avoided curve crossings; the shapes of the HF bands differ dramatically from the "unperturbed dispersions" encountered in the Mn derivative **1**. A strong correlation between microstates in the filled and empty HF spaces is diagnosed in the model polymer **7b**. The deformations of the $\varepsilon(k)$ curves cause a near degeneracy between the lowest, indirect gap ($(\pi/3) \rightarrow \Gamma$) and a direct excitation at $k = \pi/3c$. The two marginal microstates Γ and X in the valence band are of ligand σ character (large BB contributions). On the other side, the intermediate states in the vicinity of the top of the valence band are prevailingly of π type (with small σ amplitudes). The 1D models **7a** and **7b** should be suitable precursors both for the injection of electrons and holes as a result of the high-lying valence band (**7a**) and the low-lying conduction bands (**7a** and **7b**).

The sulfur atom in **8** leads to a magnification of the forbidden energy gap. The positions of the valence and conduction bands should allow the injection of holes and electrons; both "hypothetical" conductors would be organic metals with charge carriers localized in the ligand framework. Small ΔE parameters in spite of the four carbon centers per ligand ring are predicted in the 1D stacks **9a** and **9b** with 14 valence electrons (Ni 3d and ligand π) per unit cell. This surplus leads to highly populated Ni $3d_{xz}$ states in the valence bands of the Ni polymers. The associated CO wave function is neither a pure ligand orbital nor a strongly metal-centered 3d function. Both domains are important in transfer processes due to injected holes (Ni $3d_{xz}$ admixtures) or injected electrons (Ni $3d_{yz}$). Schematic representations of the Γ and X amplitudes of the valence band as well as of the conduction band are given in Figure 23. The eclipsed pattern is characterized by significant Ni $3d_{yz}$ admixtures in the conduction band. The $\varepsilon(k)$ plots of **9a** and **9b** (Fig. 17) show once again the mutual symmetry between the dispersion curves in the $\alpha = 0°$ and $\alpha = 180°$ conformations. The indirect gap in **9a** is of the $\Gamma \rightarrow$ X type, the opposite X $\rightarrow \Gamma$ excitation is found in **9b**. Thus both geometries would allow insulator-to-metal transitions with reduced lattice spacings. Strongly perturbed $\varepsilon(k)$ curves are absent in the two Ni model polymers. The energetic positions of the valence and conduction bands should

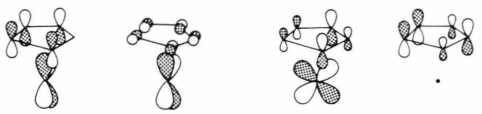

Fig. 23. Schematic representation of the crystal orbital amplitudes of the conduction (c) and valence (v) bands at the center of the Brillouin zone (ZC) and the edge of the zone (ZE) in the eclipsed Ni polymer **9a**.

allow the design of hole conductors as well as of electron transfer systems.

The additional electrons in the Ni stack **9** diminish on one side the spacing between the filled and unfilled one-particle spaces significantly. On the other side, however, the stabilizing intercell energy is reduced by ca. 20%; the mutual coupling energies amount to 16.57 eV (**9a**) and 15.91 eV (**9b**), respectively. The difference between **9a** and **9b** is due to the covalent resonance energies encountered for the nearest neighbour's interactions. The eclipsed arrangement is stabilized by means of through-space and through-bond terms between the boron atoms.

The enlarged overlap integrals in the tetraborinato Cu stacks are the origin for strongly perturbed dispersion curves with microstates, that are often modified as a function of the k-vector. π and σ states are calculated for the valence and conduction bands of the 1D backbones. The low-lying acceptor levels would suggest to dope the material with electron donors.

A vanishing band gap is predicted in the Zn stack **11**. It must be mentioned, however, that this result can not be transferred without any precaution to real solids, as the creation of a finite band gap is possible by means of a Peierls distortion [90]. In any case it should be clear that **11** is a hypothetical model, where electrical conductivities either due to injected charge carriers or due to external pressure (intrinsic conductor, i.e. overlapping bands) can be expected most probably. The extremely broad (overlapping) bands (see Table 1) allow conduction processes that are similar to the transport of free electrons (electron-lattice interactions neglected). The largest calculated band width in **11** amounts to 9.38 eV. The microstates at the top of the band are of ligand π character (π descendant of a_1 symmetry). This π dispersion has a forbidden crossing with the Zn $3d_{z^2}$ curve, which belongs to the same irreduc-

ible representation. The strong perturbations of the two $\varepsilon(k)$ curves in the crossing region is clearly seen in Figure 19. The most stable π states (a_1 symmetry) are predicted at ca. -25 eV (lowest dispersion curve in Figure 19). The "net $\pi(a_1)$ width" in the 1D stack **11** thus amounts to about 18.8 eV (compared to 8.4 eV in the cyclopentadienyl derivative **1**).

The enhanced covalent interactions (i.e. the enlarged overlap integrals) between boron centers in comparison to carbon atoms are therefore clearly demonstrated by means of the differences in the widths of the $\pi(a_1)$ bands in **11** and **1**, respectively. The broadening results from the superposition of two effects. The larger BB separations within the fivemembered ligand rings allow a reduction in the distance between the transition metal side and the plane of the π moiety. The contraction of the interplanar spacing is of course not only accompanied by a strengthening of the metal-ligand coupling, but also by a magnification of the direct (through-space) interaction between neighbouring ligand units. This geometrical enhancement effect is furthermore supported due to the diffuse valence orbitals at the B centers.

5. Conclusions

It was the purpose of the present systematic crystal orbital investigation on one-dimensional poly-decker sandwich compounds to understand those structural and geometrical factors that lead to small or vanishing band gaps in organometallic 1D stacks with 3d centers as central units and an alternating metal-ligand arrangement. Furthermore we wanted to make plain the differences between organic metals on one side and typical 3d conductors on the other side. The general trends within the computational findings can be transferred to structurally related transition metal backbones that crystallize in perpendicular stacks with the aforementioned metal-ligand-metal arrangement. On the basis of the material derived in the last two paragraphs it is possible to formulate general principles that can be used to guide synthetic activities in the area of conducting low-dimensional materials formed by organometallic building blocks:

a) Conducting 3d spines can be expected in complexes with transition metal centers from the left side of the 3d series (e.g., Ti, V, Cr, Mn, Fe), while transition metal centers with higher ionization potentials (e.g., Co, Ni, Cu, Zn) are usually not involved in conduction processes in extended organometallic materials. The conductive pathways are formed by the diffuse ligand states of the organic moieties.

b) Charge transfer processes in narrow 3d bands (hole transport) can not be described in terms of a band structure picture. Violations of the full translational symmetry (i.e. localization of the 3d hole-states) lead to a (thermally activated) hopping conductivity. The coupling to lattice vibrations is a necessary condition for this type of charge transport.

c) Hopping conductivities between localized 3d states are not restricted to 1D materials with metal-ligand-metal contacts. The 3d band widths in class **A** materials exceed only slightly the $\Delta\varepsilon$ figures in transition metal backbones belonging to the groups **B**, **C** or **D**, respectively (see Fig. 1) [24–28]. The $\Delta\varepsilon$ spectrum associated to the transition metal states in 1D materials with a metal-over-metal arrangement is prevailingly caused by k-dependent metal-ligand interactions within the unit cells of the 1D backbones or between neighbouring molecular moieties. Broad transition metal bands are only encountered in 5d materials (e.g. Krogmann's salt), where the overlap between the metal atoms is dramatically enlarged [91]. Only these materials are characterized by a significant graduation between σ, π and δ bands.

d) The model calculations have shown that the energetic separations between the filled and empty Fermi seas are reduced with an increasing number of atoms that are either less electronegative than carbon or that allow a more efficient (covalent) overlap between the ligand atoms or between the transition metal sides and the organic π centers. Therefore molecular precursors containing atomic centers from the third periode (e.g. replace C or N against Si or P) should be taken into account. Alternatively, atomic species that are found at the left of the group IV elements should be employed in synthetic routes. This means that a hydrocarbon complex should be replaced by an isovalent system where the number of 3d electrons has been enlarged while the number of electrons from the organic ligand has been reduced. Stable hydrocarbon ligands are not the optimum choice for suitable synthetic building stones associated to (intrinsic) 1D conductors.

e) Electropositive elements lead to an upward shift of the valence band(s) and to a downward shift of the conduction band(s). This facilitates the injection of charge carriers (holes and electrons) and favours furthermore the formation of photoconducting systems with thermally activated charge carriers.

f) Phase transitions (e.g. insulator-to-metal transition) are possible under pressure in a large number of 1D materials. The different $\varepsilon(k)$ profiles discussed in this context have shown that the conditions and the types of these transitions can be partially controlled by suitable substitution patterns in the organic ligands.

g) It has been demonstrated that the magnitude of the forbidden band gap depends critically on the mutual orientation of the molecular building stones. Geometry-dependent ΔE variations that exceed 2 eV have been predicted. The proper implementation of heterocenters or bulky side groups thus allows remarkable modifications of the electronic properties of the low-dimensional materials.

Acknowledgements

This work has been supported by the Stiftung Volkswagenwerk. Various discussions with Prof. W. Siebert are gratefully acknowledged. The author is grateful to Dr. W. Borrmann for critically reading the manuscript and to Mrs. I. Grimmer for her help in the preparation of the text.

[1] E. P. Goodings, Chem. Soc. Rev. **5,** 91 (1976); J. S. Miller and A. J. Epstein, Prog. Inorg. Chem. **20,** 1 (1976); A. D. Yoffe, Chem. Soc. Rev. **5,** 51 (1976).
[2] J. A. Ibers, L. J. Pace, J. Martinsen, and B. M. Hoffman, Struct. Bonding **50,** 1 (1982); B. M. Hoffman and J. A. Ibers, Acc. Chem. Res. **16,** 15 (1983).
[3] J. T. Devresse, R. P. Evrard, and V. E. van Doren (ed.), Highly Conducting One-Dimensional Solids, Plenum Press, New York 1979; W. A. Hatfield (ed.), Molecular Metals, Plenum Press, New York 1979; L. Alcaćer (ed.), The Physics and Chemistry of Low Dimensional Solids, D. Reidel Publ. Co., Dordrecht-Boston 1980.
[4] H. J. Keller (ed.), Low-Dimensional Cooperative Phenomena, Plenum Press, New York 1975; H. J. Keller (ed.), Chemistry and Physics of One-Dimensional Metals, Plenum Press, New York 1978; H. J. Keller, in: Mixed Valence Compounds, D. B. Brown (ed.), D. Reidel Publ. Co., Dordrecht-Boston 1980.
[5] H. Endres, H. J. Keller, R. Lehmann, A. Poveda, H. H. Rupp, and H. van de Sand, Z. Naturforsch. **32b,** 516 (1977).
[6] K. Krogmann, Angew. Chem. **81,** 10 (1969); M. J. Rice and J. Bernasconi, J. Phys. F: Met. Phys. **3,** 55 (1973).
[7] F. Götzfried, W. Beck, A. Lerf, and A. Sebold, Angew. Chem. **91,** 499 (1979).
[8] K. F. Schoch, B. R. Kundalkar, and T. J. Marks, J. Amer. Chem. Soc. **101,** 7071 (1979).
[9] F. Kubel and J. Strähle, Z. Naturforsch. **36b,** 441 (1981); J. Metz and M. Hanack, Nouv. J. Chim. **5,** 541 (1981); O. Schneider, J. Metz, and M. Hanack, Angew. Chem. **94,** 68 (1982); J. Metz, G. Pawlowski, and M. Hanack, Z. Naturforsch. **38b,** 378 (1983).
[10] M. Hanack and G. Pawlowski, Naturwiss. **69,** 266 (1982).
[11] H. J. Lorkowski, Top. Curr. Chem. **9,** 207 (1967).
[12] D. O. Cowan, C. LaVanda, J. Park, and F. Kaufman, Acc. Chem. Res. **6,** 1 (1973).
[13] M. Hanack, F. F. Seelig, and J. Strähle, Z. Naturforsch. **34a,** 983 (1979).
[14] F. F. Seelig, Z. Naturforsch. **34a,** 986 (1979).
[15] F. F. Seelig, Z. Naturforsch. **37a,** 1158 (1982).
[16] N. F. Mott, Proc. Phys. Soc. London **A62,** 416 (1949); J. C. Slater, Phys. Rev. **82,** 538 (1951).
[17] N. F. Mott, Metal-Insulator Transitions, Taylor and Francis, London 1974.
[18] M. C. Böhm, Theor. Chim. Acta **62,** 351 (1983).
[19] T. E. Peacock and R. McWeeny, Proc. Phys. Soc. London **74,** 385 (1959).
[20] J. M. André, L. Gouverneur, and G. Leroy, Int. J. Quantum Chem. **1,** 451 (1967); G. del Re, J. Ladik, and G. Biczó, Phys. Rev. **155,** 997 (1967).
[21] M. C. Böhm and R. Gleiter, Theor. Chim. Acta **59,** 127, 153 (1981).
[22] M. C. Böhm and H. Vogler, Solid State Commun. **46,** 201 (1983); M. C. Böhm and H. Vogler, Phys. Lett. **96A,** 41 (1983).
[23] M. C. Böhm and H. Vogler, Phys. Rev. B **28,** 3342 (1983).
[24] M. C. Böhm, Theor. Chim. Acta **62,** 373 (1983).
[25] M. C. Böhm, J. Phys. C: Solid State Phys. **16,** 1631 (1983).
[26] M. C. Böhm, Solid State Commun. **45,** 117 (1983); M. C. Böhm, Int. J. Quantum Chem., in press.
[27] M. C. Böhm, Phys. Lett. **94A,** 371 (1983); M. C. Böhm, J. Phys. C: Solid State Phys., in press.
[28] M. C. Böhm, Phys. Rev. **B 28,** 6914 (1983).
[29] M. C. Böhm, Z. Phys. Chem. N. F. **133,** 25 (1982); M. C. Böhm, Physica B, in press.
[30] M. C. Böhm, Physica **122 B,** 302 (1983).
[31] M. C. Böhm, Chem. Phys. **76,** 1 (1983).
[32] M. C. Böhm, Phys. Lett. **99 A,** 239 (1983); M. C. Böhm, Chem. Phys., in press.
[33] M. C. Böhm, Phys. Lett. **93A,** 205 (1983); M. C. Böhm, J. Chem. Phys., in press.
[34] R. G. Parr, The Quantum Theory of Molecular Electronic Structure, Benjamin, New York 1963.
[35] B. H. Brandow, Int. J. Quantum Chem. **15,** 207 (1979); K. F. Freed, Acc. Chem. Res. **16,** 137 (1983).
[36] J. Friedel, in: The Physics of Metals. 1. Electrons, M. Ziman (ed.), Cambridge University Press, Cambridge 1969.
[37] J. Friedel and C. M. Sayers, J. Phys. Paris **38,** 697 (1977).
[38] H. P. Kelly, Phys. Rev. **131,** 690 (1963); H. P. Kelly, Adv. Chem. Phys. **14,** 129 (1969).
[39] W. Hunt and W. A. Goddard, Chem. Phys. Lett. **3,** 414 (1969).

[40] W. Siebert, Adv. Organomet. Chem. **18,** 301 (1980) and references cited therein; W. Siebert, in: Transition Metal Chemistry, A. Müller and E. Diemann (ed.), Verlag Chemie, Weinheim 1981 and references cited therein. W. Siebert, Nachr. Chem. Techn. Lab. **25,** 597 (1977).
[41] J. Edwin, M. Bochmann, M. C. Böhm, D. E. Brennan, W. E. Geiger, C. Krüger, J. Pebler, H. Pritzkow, W. Siebert, W. Swiridoff, H. Wadepohl, J. Weiss, and U. Zenneck, J. Amer. Chem. Soc. **105,** 2582 (1983).
[42] W. Siebert, J. Edwin, H. Wadepohl, and H. Pritzkow, Angew. Chem. **94,** 148 (1982).
[43] M. C. Böhm, Ber. Bunsenges. Phys. Chem. **85,** 755 (1981).
[44] M. Elian and R. Hoffmann, Inorg. Chem. **14,** 365 (1975); M. Elian, M. M. L. Chen, D. M. P. Mingos, and R. Hoffmann, Inorg. Chem. **15,** 1148 (1976).
[45] J. W. Lauher, M. Elian, R. Summerville, and R. Hoffmann, J. Amer. Chem. Soc. **98,** 3219 (1976).
[46] J. Ladik and S. Suhai, in: Molecular Interactions, W. J. Orville-Thomas and H. Ratajack (ed.), Wiley Interscience, New York 1980; J. Ladik and S. Suhai, in: Theoretical Chemistry, Vol. **4,** C. Thomson (ed.), Roy. Soc. Chem., London 1981.
[47] M. Kertész, J. Koller, and A. Ažman, in: Recent Advances in the Quantum Theory of Polymers, Lecture Notes in Physics, Vol. **113,** Springer-Verlag, Berlin 1980; M. Kertész, Adv. Quantum Chem. **15,** 161 (1982).
[48] D. W. Bullett, in: Solid State Physics, Vol. **35,** H. Ehrenreich, F. Seitz, and D. Turnbull (ed.), Academic Press, New York 1980.
[49] J. C. Slater, Quantum Theory of Molecules and Solids, Vol. **4,** McGraw Hill, New York 1974.
[50] J. A. Pople and D. L. Beveridge, Approximate Molecular Orbital Theory, McGraw Hill, New York 1970.
[51] N. W. Ashcroft and N. D. Mermin, Solid State Physics, Holt, Rinehart and Winston, New York 1976.
[52] H. Fröhlich, H. Pelzer, and S. Zienau, Phil. Mag. **41,** 221 (1950); T. Holstein, Ann. Phys. **8,** 343 (1959).
[53] S. T. Pantelides, D. J. Mickish, and A. B. Kunz, Phys. Rev. B **10,** 2602 (1974).
[54] A. B. Kunz, Phys. Rev. B **12,** 5890 (1975); A. B. Kunz and D. L. Klein, Phys. Rev. B **17,** 4614 (1975).
[55] A. B. Kunz, Phys. Rev. B **26,** 2056 (1982).
[56] A. Zunger and A. J. Freeman, Phys. Rev. B **16,** 2901 (1977).
[57] T. Koopmans, Physica **1,** 104 (1933).
[58] M. C. Böhm, Theor. Chim. Acta **61,** 539 (1982); M. C. Böhm, J. Phys. B: At. Mol. Phys., in press.
[59] M. C. Böhm, J. Chem. Phys. **78,** 7044 (1983).
[60] M. C. Böhm and R. Gleiter, J. Comput. Chem. **3,** 140 (1982).
[61] C. Cauletti and I. Furlani, Struct. Bonding **35,** 119 (1980); J. C. Green, Struct. Bonding **43,** 37 (1981).
[62] M. C. Böhm, R. Gleiter, F. Delgado-Pena, and D. O. Cowan, J. Chem. Phys. **79,** 1154 (1983).
[63] P. A. Cox, M. Benard, and A. Veillard, Chem. Phys. Lett. **87,** 159 (1982); M. Benard, Theor. Chim. Acta **61,** 379 (1982); M. D. Newton, Chem. Phys. Lett. **90,** 291 (1982); M. Benard, Chem. Phys. Lett. **96,** 183 (1983).
[64] D. Post and E. J. Baerends, Chem. Phys. Lett. **86,** 176 (1982); R. P. Messmer, T. C. Caves, and C. M. Kao, Chem. Phys. Lett. **90,** 296 (1982).
[65] A. B. Kunz, in: Excited States in Quantum Chemistry, C. A. Nicolaides and D. R. Beck (ed.), D. Reidel Publ. Co., Dordrecht-Boston 1979.
[66] L. Noodleman and J. G. Norman, J. Chem. Phys. **70,** 4903 (1979); J. G. Norman, P. Barry-Ryan, and L. Noodleman, J. Amer. Chem. Soc. **102,** 4279 (1980).
[67] M. Benard, J. Chem. Phys. **71,** 2546 (1979).
[68] M. C. Böhm, Theor. Chim. Acta **60,** 233 (1981); M. C. Böhm, Mol. Phys. **46,** 255 (1982).
[69] M. C. Böhm, Int. J. Quantum Chem. **24,** 185 (1983).
[70] M. C. Böhm, J. Phys. B: At. Mol. Phys. **16,** L397 (1983).
[71] S. Suhai, Phys. Rev. B **27,** 3506 (1983).
[72] M. C. Böhm, Int. J. Quantum Chem., submitted for publication.
[73] A. B. Kunz and G. T. Surratt, Solid State Commun. **25,** 9 (1978).
[74] A. B. Kunz, R. S. Weidman, J. Boettger, and G. Cochran, Int. J. Quantum Chem. **S 14,** 585 (1980).
[75] J. Brust, Methods in Computational Physics, Vol. 8, Academic Press, New York 1968; J. Delhalle, in: Electronic Structure of Polymers and Molecular Crystals, J. M. André and J. Ladik (ed.), Plenum Press, New York 1975.
[76] D. R. Hartree, The Calculation of Atomic Structures, John Wiley, New York 1957.
[77] E. Dubler, M. Textor, H.-R. Oswald, and A. Salzer, Angew. Chem. **86,** 125 (1974); W. Siebert, G. Augustin, R. Full, C. Krüger, and Y.-H. Tsay, Angew. Chem. **87,** 286 (1975); W. Siebert, T. Renk, K. Kinberger, M. Bochmann, and C. Krüger, Angew. Chem. **88,** 850 (1978); W. Siebert, C. Böhle, C. Krüger, and H.-Y. Tsay, Angew. Chem. **90,** 558 (1978); W. Rothermel, C. Böhle, C. Krüger, and D. J. Brauer, Angew. Chem. **91,** 1014 (1979).
[78] W. Siebert, J. Edwin, and H. Pritzkow, Angew. Chem. **94,** 147 (1982); W. Siebert, private communications.
[79] L. E. Sutton (ed.), Tables of Interatomic Distances and Configuration in Molecules and Ions, Spec. Publ. No. 18, The Chemical Society, London 1965.
[80] A. Haaland, Acc. Chem. Res. **12,** 415 (1979).
[81] P. Seiler and J. D. Dunitz, Acta Cryst. **B 35,** 1068 (1979).
[82] D. W. Clack and K. D. Warren, Inorg. Chem. **18,** 513 (1979); D. W. Clack and K. D. Warren, J. Organomet. Chem. **208,** 183 (1981).
[83] M. C. Böhm, M. Eckert-Maksić, R. Gleiter, G. E. Herberich, and B. Hessner, Chem. Ber. **115,** 754 (1982).
[84] M. C. Böhm, Z. Naturforsch. **37 a,** 1193 (1982).
[85] P. S. Bagus, U. I. Wahlgren, and J. Almlöf, J. Chem. Phys. **64,** 2324 (1976); J. H. Ammeter, H.-B. Bürgi, J. C. Thibeault, and R. Hoffmann, J. Am. Chem. Soc. **100,** 3686 (1978); H. P. Lüthi, J. H. Ammeter, J. Almlöf, and K. Faegri, Jr., J. Chem. Phys. **77,** 2002 (1982).
[86] M.-M. Rohmer, J. Demuynck, and A. Veillard, Theor. Chim. Acta **36,** 93 (1974).
[87] J. Martinsen, L. J. Pace, T. E. Phillips, B. M. Hoffman, and J. A. Ibers, J. Amer. Chem. Soc. **104,** 83 (1982).
[88] M. W. Whiteley, H. Pritzkow, U. Zenneck, and W. Siebert, Angew. Chem. **94,** 464 (1982).
[89] M. C. Böhm, manuscript in preparation.
[90] R. E. Peierls, Quantum Theory of Solids, Clarendon Press, London 1955.
[91] R. P. Messmer and D. R. Salahub, Phys. Rev. Lett. **35,** 533 (1975); H. Yersin, G. Gliemann, and U. Rössler, Solid State Commun. **21,** 915 (1978); D. W. Bullett, Solid State Commun. **27,** 915 (1978); M.-H. Whangbo and R. Hoffmann, J. Amer. Chem. Soc. **100,** 6093 (1978).